The mitochondrial OXidation Resistance protein AtOXR2 increases plant biomass and tolerance to oxidative stress.

Francisco Colombatti[1a], Regina Mencia[1a], Lucila Garcia[1,2], Natanael Mansilla[1], Sergio Alemano[3], Andrea M. Andrade[3,4], Daniel H. Gonzalez[1] and Elina Welchen[1]*

[1]Instituto de Agrobiotecnología del Litoral (CONICET-UNL), Cátedra de Biología Celular y Molecular, Facultad de Bioquímica y Ciencias Biológicas, Universidad Nacional del Litoral, 3000 Santa Fe, Argentina

[2]Instituto de Biología Molecular y Celular de Rosario (IBR-CONICET), Rosario, Argentina.

[3]Laboratorio de Fisiología Vegetal. Universidad Nacional de Río Cuarto, 5800 Río Cuarto, Córdoba, Argentina.

[4]Consejo Nacional de Investigaciones Científicas y Técnicas (CONICET).

[a]Both authors contributed equally to this work. Listed in alphabetical order.

***Correspondence:**

Elina Welchen, Instituto de Agrobiotecnología del Litoral (CONICET-UNL), Centro Científico Tecnológico CONICET Santa Fe, Colectora Ruta Nac. Nº 168 km 0, Paraje el Pozo s/n, 3000 Santa Fe, Argentina. Phone: +54-342-4511370 (5022) e-mail: ewelchen@fbcb.unl.edu.ar

Author E-mails: Francisco Colombatti: francisco.colombatti@molinosagro.com.ar; Regina Mencia: rmencia@santafe-conicet.gov.ar; Lucila Garcia: garcia@ibr-conicet.gov.ar; Natanael Mansilla: nmansilla@fbcb.unl.edu.ar; Sergio Alemano: salemano@exa.unrc.edu.ar; Andrea M. Andrade: aandrade@exa.unrc.edu.ar; Daniel Gonzalez: dhgonza@fbcb.unl.edu.ar; Elina Welchen: ewelchen@fbcb.unl.edu.ar.

Highlight:

The Oxidation Resistance family protein AtOXR2 from *Arabidopsis thaliana* is involved in resistance to oxidative stress and its overexpression increases plant biomass, seed production and photosynthetic performance.

ABSTRACT

The study described here demonstrates the existence of the OXidation Resistance (OXR) protein family in plants. There are six OXR members in Arabidopsis that contain the highly conserved TLDc domain that is characteristic of this eukaryotic protein family. AtOXR2 is a mitochondrial protein able to alleviate the stress sensitivity of a yeast *oxr1* mutant. AtOXR2 is induced by oxidative stress. AtOXR2 overexpression in Arabidopsis (oeOXR2) increases leaf ascorbate, photosynthesis, biomass and seed production, as well as conferring tolerance to methyl viologen, antimycin A and high light intensities. The oeOXR2 plants also show higher ABA content, changes in ABA sensitivity and modified expression of ABA- and stress-regulated genes. While the *oxr2* mutants have a similar shoot phenotype to the wild type, they exhibit increased sensitivity to stress. We propose that by influencing the levels of reactive oxygen species (ROS) AtOXR2 improves the efficiency of photosynthesis and elicits basal tolerance to environmental challenges that increase oxidative stress, allowing improved plant growth and biomass production.

Keywords:

OXR family, TLDc domain, mitochondria, plant biomass, ROS, ABA, oxidative stress.

Abbreviations:

AA, Antimycin; CLSM, confocal laser scanning microscopy; DAS, days after sowing; DAB, 3,3′-diaminobenzidine; ETR, electron transport rate; GUS, β-glucuronidase; HL, high light; LD, long day; MV, methylviologen; mRFP, monomeric red fluorescent protein; mt-GFP, GFP in mitochondria; OMM, mitochondrial outer membrane; PPFD, photosynthetically active photon flux density; ROS, reactive oxygen species; RT-qPCR, reverse transcription quantitative real-time PCR; PS, Photosystem; SAA, systemic acquired acclimation; WT, wild-type.

Introduction

In addition to energy, normal aerobic metabolism in eukaryotic cells generates reactive oxygen species (ROS). At homeostatic levels, ROS act as signalling molecules responsible to orchestrate numerous cellular activities related to posttranslational protein modifications, gene expression, and hormonal regulation (Foyer *et al*., 2017; Mittler, 2017). When ROS levels surpass the cellular buffering ability, they become dangerous compounds due to their enormous reactivity and potential to generate protein, lipid and DNA damage (Czarnocka and Karpiński, 2018). As cells evolved into aerobic metabolism, they also strengthened defence mechanisms to avoid or alleviate the consequences of oxidative damage caused by excess ROS (Noctor *et al*., 2017). Due to respiratory activity and electron flow, mainly through complexes I, II and III of the electron transport chain, mitochondria are one of the main sites of ROS generation (Gleason *et al*., 2011; Jardim-Messeder *et al*., 2015). In plant mitochondria, there are energy decoupling systems represented by the alternative oxidase (Vanlerberghe, 2013) and the uncoupling proteins (Vercesi *et al.,* 2006). Plant mitochondria also acquired numerous antioxidant pathways based on proteins with thioredoxin, glutaredoxin, peroxiredoxin and superoxide dismutase (SOD) activities (Navrot *et al.,* 2007; Cvetkovska *et al*., 2012; Foyer and Noctor, 2016; Dietz *et al*., 2016; Liebthal *et al*., 2017).

Among the efforts to elucidate the defence lines used by human cells to counteract oxidative damage and its consequences, a new family of eukaryotic proteins called OXR (*Oxidation Resistance*) was identified (Volkert *et al*., 2000). The most highly conserved region of OXR proteins across species is the carboxyl-terminal half, which contains a TLDc (*T*BC (*Tre2/Bub2/Cdc16*), *L*ysM (Lysine Motif), *D*omain *c*atalytic) domain (IPR006571, PF07534, SM00584). This is a novel protein domain that was predicted to have enzymatic properties (Doerks *et al*., 2002) and, according to X-ray crystallographic studies of the TLDc domain of OXR2 from zebrafish, adopts an overall globular shape that shares no similarity with other known structures (Blaise *et al.*, 2012).

There are studies of OXR proteins in yeast (Elliott and Volkert, 2004), *D. melanogaster* (Stowers *et al*., 1999; Wang *et al*., 2012; 2013), *Anopheles* (Jaramillo-Gutierrez *et al*., 2010), mouse (Fischer *et al.*, 2001; Natoli *et al.*, 2008; Oliver *et al.*, 2011; Wu *et al.*, 2016), zebrafish (Laroche *et al.*, 2013; Kobayashi *et al.*, 2014), *C. elegans* (Sanada *et al.*, 2014), silkworms (Su *et al*., 2017) and humans (Volkert *et al.*, 2000; Elliott and Volkert, 2004; Durand *et al.*, 2007; Shkolnik *et al.*, 2008; Yang *et al.*, 2014; Liu *et al.*, 2015; Finelli *et al.*, 2016). Although the mechanism by which OXR proteins exert their action is still unknown, the TLDc domain was implicated in the prevention of oxidative DNA damage (Elliott and Volkert, 2004; Durand *et al.*, 2007) and in the

induction of antioxidant enzymes (Jaramillo-Gutierrez *et al.*, 2010; Su *et al.*, 2017). Disruption of TLDc-encoding genes originates a decrease in lifespan in mice (Oliver et al., 2011, *Drosophila* (Fischer *et al.*, 2001), nematodes (Sanada *et al.*, 2014) and mosquitoes (Jaramillo-Gutierrez *et al.*, 2010), or causes severe neurological disorders in humans (Finelli *et al.*, 2016; Wu *et al.*, 2016). Mutations in the TLDc domain of the human gene *TBC1C24* affect brain development and generate DOORS (Deafness, Onychodystrophy, Osteodystrophy, mental Retardation and Seizures) syndrome (Campeau *et al.*, 2014).

There is scarce evidence about the role of TLDc domain-containing proteins in plants. Only a study by Lin and co-workers (2012) showed that *IbTLD* from sweet potato is one of the targets of the wounding-induced microRNA *miR828*, which regulates the expression of antioxidant enzymes and defence responses against abiotic stress. Due to the relevance of different TLDc-containing proteins in several eukaryotic organisms (Finelli *et al.*, 2016), we decided to analyse the presence and role of proteins belonging to the OXR family in Arabidopsis. In this work, we identified six genes that encode members of the OXR family in Arabidopsis and characterised At*OXR2* (At2g05590) in more detail. We observed that AtOXR2 is a mitochondrial protein that can functionally replace its yeast Oxr1p homologue. When AtOXR2 is absent it generates a plant phenotype of decreased tolerance to oxidative stress conditions. Besides, plants that overexpress AtOXR2 show improved photosynthesis, increased biomass and changes in oxidative stress tolerance and ABA sensitivity.

Materials and methods

Plant material and growth conditions

Arabidopsis thaliana (Col-0) was used throughout this study unless otherwise specified. The At*OXR2* T-DNA insertion mutant line SK17762 and Flag_513D06 (ecotype WS) were used. Plants were grown on soil at 22-24ºC under long-day (LD) conditions at intensity of 100 µmol m^{-2} s^{-1}. Plant phenotypic characterization was performed according to the parameters established by Boyes *et al.* (2001), using ten individual plants of each genotype per biological triplicate.

Gene cloning and generation of transgenic Arabidopsis lines for plant transformation

To obtain plants expressing a fusion of AtOXR2 to mRFP or GFP, a 912-bp *Bgl*II/*Xho*I fragment was amplified from a cDNA clone (RAFL06-07-C06) using specific oligonucleotides (Table S1) and transferred to the destination binary vectors pGWB554 (Nakagawa *et al.*, 2007) or pEarleyGate103 (Earley *et al.*, 2006). To obtain plants that constitutively overexpress At*OXR2* under the control of the CaMV *35S* promoter (oeOXR2 plants), a 912-bp *Bam*HI/*Xho*I fragment

was transferred into destination vector pEarleyGate100 (Earley *et al.*, 2006). To obtain Arabidopsis plants expressing At*OXR2* promoter:*GUS* fusions, a fragment spanning nucleotides -1157 to +95 relative to the transcription start site was cloned into binary vector pBI101.3. β-glucuronidase (GUS) activity in protein extracts was measured as described by Jefferson *et al.* (1987). For plant transformation, *Agrobacterium tumefaciens* strain LBA4404 transformed with the respective constructs was used to obtain transgenic Arabidopsis plants by the floral dip procedure (Clough and Bent, 1998). Fifteen positive independent lines for each construct were used to select homozygous T3 and T4 plants in order to analyse phenotypes and expression levels.

Complementation of an *oxr1* yeast mutant with At*OXR2*

For complementation of the *S. cerevisiae oxr1* mutant, a fragment comprising the entire At*OXR2* coding sequence was amplified from cDNA clone RAFL06-07-C06, fused to a fragment encoding the mitochondrial targeting sequence (MTS) of yeast Sod2p (Elliott and Volkert, 2004) and cloned into yeast expression vector pMV611 (Wang *et al.*, 2004). Constructs with the insert and the empty plasmid were introduced into the yeast *oxr1* strain BY4742/*oxr1* by using the standard lithium acetate transformation method. Sensitivity to H_2O_2 was assayed as described by Elliott and Volkert (2004).

Confocal Laser Scanning Microscopy (CLSM)

For CLSM, roots and leaves of 15-day-old plants containing the 35S:AtOXR2-mRFP construct in the *mt-gk* background (Nelson *et al.*, 2007) were imaged with a Leica TCS SP8 or a Zeiss LSM880 confocal laser scanning microscope with excitation at 488 nm and detection at 498-531 nm for GFP. The excitation of mRFP was accomplished with the 561-nm laser line, and the emission was detected between 587 and 620 nm. Chlorophyll and presence of chloroplast were recorded at 633-nm laser excitation line with emission at 650 to 600 nm. Parameters were set according to Wagner *et al.*, (2015). For colocalisation analysis, intensity-scatter plots were generated with the "Coloc 2" and "Colocalisation Threshold" plugins of the Fiji software (Schindelin *et al.*, 2012).

Analysis of AtOXR2 localization by Western blot

Analysis of AtOXR2 mitochondrial localization by Western blot was performed according to Steinebrunner *et al.* (2011) with slight modifications. Mitochondria enriched proteins extracts and subcellular fractions were prepared from aerial parts of 20-day-old fully expanded rosette leaves of Arabidopsis plants carrying the 35S:AtOXR2-GFP construct. Briefly, leaf

homogenates were first centrifuged at 2500 *g* for 5 min to obtain a fraction enriched in chloroplasts (fraction I). The supernatant was then centrifuged at 15000 g for 15 min. The pellet was resuspended and the procedure described above was repeated to obtain a fraction enriched in mitochondria. The supernatant of this centrifugation, containing soluble proteins and small vesicles, is referred to as fraction II. For Western blot analysis, protein fractions were loaded in a 15% SDS gels and transferred to a PVDF membrane (GE Healthcare). Blots were incubated with polyclonal rabbit antibodies against GFP (Abcam #ab290) at a dilution of 1:5000, cytochrome *c* oxidase subunit 2 (COX2, Agrisera #AS04 053A), plastocyanin (a gift of Dr. Marinus Pilon, Colorado State University) at a dilution of 1:500, and actin (Agrisera #AS132640) at 1:10000 dilution. Reactions were developed with 1:20000 Goat anti-Rabbit IgG (H&L), HRP conjugated (Agrisera, #AS09 602) using the Agrisera ECL kit (AS16 ECL-SN).

Stress treatments

For UV-B (5 mW/cm^2; UVP 34-0042-01 lamp) and high light (HL) (600 µmol m^{-2} s^{-1}) exposure, whole rosettes of 3-week-old plants grown on soil were used. For 3-aminotriazol (3-AT) treatments, detached leaves were placed on a 4 mM 3-AT solution. Photosynthetic parameters of plants exposed to HL were measured on full expanded leaves after 24-72 hours of treatment. For methylviologen (MV) treatments, seedlings were grown on MS-agar medium supplemented with 0.1 µM MV. Plates were vertically set and root length was recorded every day. For Antimycin A (AA) treatment, 2-week-old seedlings were transferred to MS medium supplemented with 50 µM AA and harvested in biological triplicate at 1 and 3 h after treatment. For analysis of gene expression, samples were immediately frozen in liquid nitrogen and stored at -80°C until use.

RNA isolation and analysis

RNA samples were prepared with TRIZOL RNA Isolation Reagent (Life Technologies). RT-qPCR analysis was performed according to O'Connell (2002). Quantitative PCR was performed on an aliquot of the cDNA with specific primers (Table S1) using the StepOnePlus® Real-Time PCR System (Czechowski, 2005). For microarray analysis, RNA obtained from wild-type (WT) and oeOXR2 rosettes were hybridized in Agilent Arabidopsis (v4) Gene Expression 4x44K Microarrays using two-color reciprocal labeling. Further processing of probe intensities was performed with the R statistical programming environment (R Development Core Team, 2013) and the Limma package from the Bioconductor project (Gentleman *et al.*, 2004). Analyses of enriched biological process gene ontology (GO) terms were made using the MRCM tool (Multi-Reference Contrast Method; Fresno *et al.*, 2012). The data were deposited in NCBI's Gene

Expression Omnibus (Edgar, 2002) and are accessible through GEO Series accession number GSE114689 (https://www.ncbi.nlm.nih.gov/geo/query/acc.cgi?acc=GSE114689).

Measurement of photosynthetic parameters

Leaf photosynthetic parameters were measured using a LiCOR 6400-XT portable photosynthetic system (LI-COR Inc.). Analysis was made on the 4^{th}, 5^{th} and 6^{th} leaf pairs. Prior to measurements, each leaf was adapted for 10 min to darkness and ten measurements were made using different plants for each genotype. Chlorophyll fluorescence parameters were calculated according to Maxwell and Johnson (2000) and Baker (2008).

Histology and microscopy

Histological sections of Arabidopsis stems were obtained according to Moreno-Piovano *et al.* (2017). For microscopic visualization we used an Eclipse E200 Microscope (Nikon) equipped with a Nikon Coolpix L810 camera.

ABA identification and quantification by liquid chromatography-electrospray ionization tandem mass spectrometry (LC-ESI/MS-MS)

Abscisic acid (ABA) was extracted from 200 mg (dry weight) plant material as described by Durgbanshi *et al.* (2005). ABA was separated from plant tissues by reversed-phase HPLC, using an Alliance 2695 separation module (Waters; Milford, MA, USA) equipped with a Restek Ultra C18 3 µm column (100×3.0 mm). ABA was identified and quantified using a quadruple tandem mass spectrometer (Quattro Ultima, Micromass; Manchester, UK) fitted with an electrospray ion (ESI) source, in multiple reactions monitoring mode (MRM) using precursor ions and their transitions (m/z) to ABA (m/z 263/153) and D6-ABA (m/z 269/159). The collision energies used were 15 eV (electron volts). The cone voltage was 35V. The MassLynx spectrometry software program V. 4.1 (Waters) was used for data analysis.

Analysis of stomatal aperture

Rosette leaves were incubated under moderate light intensity (180 µmol m^{-2} s^{-1}) for 3 h. ABA was added at a final concentration of 5 µM for 1 additional hour. Then, leaf epidermal prints were obtained and placed on a slide containing 50 µL of 0.1% toluidine blue. The stomatal aperture index (SAI) was calculated as the ratio of stomata length to width (Eisele *et al.*, 2016).

Determination of lipid peroxidation

Malondialdehyde equivalents were calculated according to Hodges *et al.* (1999).

Detection of endogenous H_2O_2

Intracellular ROS levels were determined by 2',7'-dichlorodihydrofluorescein diacetate (H_2DCFDA; Molecular Probes) staining. Leaf discs were incubated for 10 min in the dark in a solution containing the probe (1 µM, pH 7.2) and washed tree times with HEPES 20 nM pH 7.2. Discs where placed on a multiwell plate and ROS levels were quantified by measuring the emitted fluorescence (538 nm) using a Thermo Scientific Fluoroskan Ascent™.

Anthocyanin and ascorbic acid measurement

Total anthocyanins were estimated following Lee *et al.* (2005) on 100 mg of leaves from plants cultivated under normal growth conditions or after exposure to HL during 3 days. Ascorbic acid content was measured in full expanded leaves of 21-day-old plants using a microplate-adapted colorimetric assay described by Gillespie and Ainsworth (2007). The results represent the mean±SE of five independent samples.

Sequence alignment and phylogenetic tree analysis

Arabidopsis OXR family members were identified using the Blastp tool (Boratyn *et al.*, 2013) and human and yeast OXR1 as query sequences. Sequence similarity (Table S2) was calculated using the Clustal Omega tool (Sievers *et al.*, 2014). Plant TLDc containing proteins were identified using the Arabidopsis family members AtOXR1 to AtOXR5 as queries. Sequences with an E-value lower than 10^{-5} (Table S3) were downloaded from Phytozome 12 (Goodstein *et al.*, 2012) and Gymno PLAZA. Sequence alignment was made using default parameters established in the WebPRANK alignment server (Löytynoja and Goldman, 2010). Phylogenetic trees were built using the Seaview 4.5.0 software and the PhyML-aLRT-SH-LIKE algorithm (G*ouy et al.*, 2010) with maximum likelihood tree reconstruction. A model of the amino acid substitution matrix was chosen through the Datamonkey bioinformatic server (www.datamonkey.org; Delpor *et al.*, 2010), which showed the WAG model. The resulting tree was represented using iTOL (http://itol.embl.de/itol.cgi; Letunic and Bork, 2016) showing branches with bootstraps higher than 70%.

Homology modeling

The AtOXR2 TLDc domain homology model was generated using the Swiss-model server (Kiefer *et al.*, 2009) using the structure of the zebrafish OXR2 (A9JTH8) TLDc domain as a reference (PDB: 4acj; Blaise *et al.*, 2012).

Statistical analysis

Data were analysed by one-way ANOVA and the means were compared by Tukey or Fisher (LSD) tests. Statistical analysis was performed using InfoStat Version 2013 for Windows (http://www.infostat.com.ar).

RESULTS

Identification and evolutionary analysis of OXR family proteins in plants.

A survey of sequences in the Arabidopsis genome with similarity to OXR proteins from yeast and humans allowed us to identify five genes coding for OXR family members: *At4g39870*, *At2g05590*, *At5g06260*, *At1g32520* and *At5g39590*, which were arbitrarily named by numbers from one to five: At*OXR1*, At*OXR2*, At*OXR3*, At*OXR4* andAt*OXR5*, respectively (Fig. 1A). The presence of a TLDc domain in the five proteins was confirmed by searches in the Pfam database (El-Gebali *et al.*, 2019). Notably, the TLDc domain of AtOXR4 is shorter and appears to be truncated (Fig. 1A). In addition, a sixth protein with high identity to AtOXR3, but with a truncated TLDc domain, was identified. This protein is encoded by gene *At4g34070* and was named AtOXR6. The TLDc domain is present in the carboxy-terminal half of the identified proteins (Fig. 1A), as previously found in family members from other organisms (Finelli *et al.*, 2016). AtOXR3 and AtOXR6 contain EF-hand calcium-binding motifs characteristic of the penta-EF hand (EFh) protein family (Maki *et al.*, 2002). Using a multiple sequence alignment (Sievers *et al.*, 2014), we obtained a percentage identity matrix of the Arabidopsis family members and the yeast and human OXR proteins (Table S2). The highest sequence identity with the human and yeast proteins was observed for AtOXR1 and AtOXR2 (26-31% for the complete proteins and 32-42% for the TLDc domains; Table S2). We used AtOXR family members to identify OXR protein sequences in different plant species that were used to build a phylogenetic tree (Table S3; Fig. 1B). The tree shows the presence of three clades (OXR1/2, OXR3/6 and OXR4) containing proteins representative from different lineages, from algae to flowering plants. A fourth clade (OXR5) contains proteins from land plants, but not from algae (Fig. 1B), suggesting that this clade may have originated by a duplication that took place early during land plant evolution. The OXR1 and OXR2 clades probably evolved later, since OXR1 and OXR2 proteins share more similarity among themselves than with the other clades. In addition, the OXR1 and OXR2 clades cannot be recognized in algae, which instead contain a more divergent clade that seems to be the ancestor of OXR1 and OXR2 (Fig. 1B; Table S4). Since proteins from *P. patens* and *S. moellendorffii* cluster together with OXR1, it is likely that the duplication that

originated OXR1and OXR2 took place during land plant evolution (Fig. 1B). OXR proteins from yeast and humans cluster together with the clade containing AtOXR1, AtOXR2 and their ancestors (Fig. 1B), in agreement with the highest similarity found between these proteins. Finally, a very recent duplication probably generated the AtOXR6 family member from AtOXR3 protein only in Arabidopsis.

Analysis of OXR2 phylogeny and structure of the TLDc domain

As a first step to evaluate the role of OXR proteins in plants, we chose AtOXR2 due to its higher sequence similarity to proteins previously identified in humans and yeast (Table S2) (Volkert *et al.*, 2000; Elliott and Volkert, 2004). First, we built a tree only with OXR2 protein sequences (Fig. S1). OXR2 proteins are present in conifers and in *Amborella trichopoda*, the most primitive angiosperm. There are representative members in monocot and dicot plants of economic impact (Fig. S1). The structure of the tree closely follows the evolution of the different species, suggesting that these proteins arise from a common ancestor. More than one OXR2 protein is present in some species, probably arising from recent duplications (Fig. S1). The AtOXR2 TLDc domain shares 40.7%, 38.8%, 35.2% and 28.4% sequence identity with human HsOXR1, zebrafish DreOXR2, drosophila DmOXR1 and yeast Oxr1p (ScOXR1), respectively (Fig. 1C), suggesting that the overall structure of its TLDc domain is conserved. Relevant amino acid residues (Gly-93, Gly-174 and Glu-216; numbering based on the human Nuclear receptor coactivator 7 (Ncoa7B) TLDc-containing protein sequence; Finelli *et al*., 2016) are conserved in AtOXR2 (arrowheads in Fig. 1C). The Gly-93 and -174 residues would be important for maintaining the structural integrity of the TLDc domain, while Glu-216 is essential for the neuroprotective function of HsOXR1 (Finelli and Oliver, 2017).

We used data provided by Blaise and co-workers (2012) related to the crystal structure of the TLDc domain of OXR2 from *Danio rerio* (DreOXR2; Uniprot: A9JTH8) to deduce the structure of the AtOXR2 TLDc domain. The DreOXR2 domain is composed of four α-helices that surround a globular core conformed by ten β-sheets (Blaise *et al.*, 2012). The AtOXR2 TLDc domain three-dimensional structure perfectly matches the previously reported structure of DreOXR2 (Fig. 1D). This domain is predicted to be a catalytic domain (Doekers *et al.*, 2000). However, in spite of the high conservation through different species, the function of the TLDc domain remains unknown (Finelli and Oliver, 2017).

AtOXR2 is localised to plant mitochondria *in vivo*

Different OXR proteins have been localised to different cell compartments, notably mitochondria, nucleus and cytoplasm (Elliott and Volkert, 2004; Durand *et al.*, 2007). *In silico* analysis of AtOXR2 shows no N-terminal subcellular targeting sequence (MitoFates; Fukasawa *et al.*, 2015) and the SUBcellular Arabidopsis consensus (SUBAcon) algorithm locates it in plastids (Hooper *et al.*, 2017). The AtOXR2 hydrophobicity profile, according to the ARAMENNON database (Schwacke *et al.*, 2003), predicts a consensus transmembrane domain spanning amino acids 236 to 256 and the presence of a putative GPI-anchor attachment signal (Fankhauser and Mäser, 2005). To obtain experimental evidence, the coding region of AtOXR2 was tagged with the mRFP coding sequence and expressed in Arabidopsis. AtOXR2-mRFP was observed in dot-shaped structures, most likely reflecting mitochondria (Fig. 2A). To confirm mitochondrial localisation, the construct expressing AtOXR2-mRFP was introduced into the Arabidopsis *mt-gk* line, which expresses GFP in mitochondria (Nelson *et al.*, 2007). Several lines co-expressing AtOXR2-mRFP and mito-GFP were analysed by CLSM showing that GFP fluorescence co-localised with the mRFP fluorescence in root and leaf cells (Fig. 2A), suggesting that AtOXR2 is a mitochondrial protein. In addition, no evidence for co-localisation of the mRFP fluorescence with chlorophyll fluorescence was obtained (Fig. 2A), ruling out a plastid localisation, at least under these conditions. In order to confirm the localisation, we performed a Western blot analysis of proteins from different subcellular fractions of rosette leaves from 20-day-old plants expressing AtOXR2-GFP. Using anti-GFP antibodies, we detected AtOXR2-GFP only in the fraction enriched in mitochondria (Fig. 2B). A similar result was obtained with antibodies against the mitochondrial protein COX2 (Fig. 2B). In turn, the chloroplast protein plastocyanin was present in the non-mitochondrial fraction (Fig. 2B). Finally, actin, a cytosolic protein, was present in both fractions, but clearly enriched in the non-mitochondrial fraction, and the same was observed in the Ponceau staining of the blot for a protein that probably corresponds to the large subunit of Rubisco (Fig. 2B). Altogether, even if plastid or cytosolic localisation in minor amounts cannot be completely ruled out, the results indicate that AtOXR2 is a mitochondrial protein. In addition, its possible presence in other organelles, like peroxisomes, will require additional studies with N-terminal fusions of the fluorescent protein.

Mitochondrial-targeted AtOXR2 alleviates the stress sensitivity of a yeast *oxr1* mutant.

There is only one OXR protein in *S. cerevisiae*, Oxr1p, which is located in mitochondria. The *oxr1* yeast mutants are 10-fold more sensitive to H_2O_2 than WT cells (Volkert *et al.*, 2000). To evaluate if AtOXR2 is able to revert the oxidative stress sensitivity of the *oxr1* mutant, we

transformed the *oxr1* (YPL106w, oxr1Δ) mutant strain with a construct expressing AtOXR2 fused to the MTS of yeast Sod2p in its N-terminal portion to ensure mitochondrial localisation in yeast, as performed by Elliot and Volkert (2004) for the human protein. In the transformants, we analysed cell viability after treatment with H_2O_2. At 150 μM, H_2O_2 significantly affected the growth of *oxr1* mutant cells (oxr1Δ), compared to WT (BY742) cells (Fig. 3). Expression of At*OXR2* was able to almost completely restore normal growth in the presence of H_2O_2 (Fig. 3), suggesting that AtOXR2 can fulfil a similar role as yeast Oxr1p in the protection from oxidative stress.

At*OXR2* is induced by abiotic stress

In order to analyse the expression pattern of At*OXR2*, we fused the *uidA* (*gus*) reporter gene to a 1252-bp fragment (-1157 to +95) corresponding to the putative At*OXR2* promoter region (p*OXR2*:*GUS*). Histochemical detection of GUS activity in ten independent Arabidopsis transformed lines revealed expression in cotyledon tips and veins, apical meristem and leaf primordia, with strong expression in trichomes (Fig. 4A, a-e). Expression was also observed in vascular tissues of roots, hypocotyls and leaves (Fig. 4Ab, d, h). In flowers, expression was detected in mature pollen grains (Fig. 4Af, g). GUS expression levels were also quantified in total protein extracts from 2-week-old Arabidopsis seedlings and in extracts prepared from different tissues of adult plants. Highest expression was observed in flowers, and comparable levels of GUS activity were detected in seedlings, rosette leaves and roots, while expression in siliques was low (Fig. 4B). Analysis of transcriptomic data available for At*OXR2* in the ePlant visualization tool (http://bar.utoronto.ca/eplant/; Waese *et al*., 2017) showed higher expression in thichomes, vascular tissue and mature pollen (Fig. S2), in agreement with the results observed with the reporter construct.

It is well known that OXR proteins from several organisms are induced under conditions that promote oxidative stress (Oliver *et al.*, 2011; Finelli *et al.*, 2016). To evaluate if this also applies to At*OXR2*, we exposed Arabidopsis WT and p*OXR2*:*GUS* plants to different stress treatments. Increased GUS activity was observed after exposure to HL intensity, UV-B light and treatments with 3-AT, conditions that increase ROS and H_2O_2 endogenous levels (Fig. 4C). Higher At*OXR2* transcript levels were also observed after treatment of WT seedlings with MV, AA and UV-B light (Fig. 4D), all conditions that generate oxidative damage.

Increased At*OXR2* expression enhances photosynthetic performance and increases plant biomass and seed production

To gain more evidence about the function of At*OXR2*, we analysed plants with altered expression of this gene. We characterized two Arabidopsis insertional knockout mutants identified as *oxr2.1* and *oxr2.2* and obtained several lines overexpressing At*OXR2* under the CaMV *35S* promoter (oeOXR2) (Fig. S3). We characterized phenotypic parameters of these plants through the whole life cycle. No differences in comparison to WT were observed for *oxr2.1* and *oxr2.2* mutant plants under normal growth conditions (Fig. 5A, B; Fig. S4). In contrast, two independent oeOXR2 lines (A and B) exhibited increased rosette diameter and area, and produced higher number of leaves and biomass compared to WT plants (Fig. 5A, B; Fig. S4). Fully expanded leaves from four-week-old oeOXR2 plants showed differences in photosynthetic parameters when compared with WT leaves at the same stage. Except for parameters of the basal fluorescence (F_s and F_o), all other fluorescence parameters were increased in leaves from overexpressing plants (Fig. S5A). As a result, the maximum Photosystem II (PSII) efficiency (Fv/Fm), the PSII efficiency (ΦPSII), and photochemical and non-photochemical quenching parameters (q_P, q_N and NPQ) were elevated in the overexpressing lines in comparison with WT plants (Fig. S5A). Moreover, oeOXR2 plants exhibited an improved photosynthetic performance and higher values of electron transport rate (ETR) in a wide range of light intensities (Fig. 5C). Analysis of gas exchange parameters showed that oeOXR2 plants exhibited an increased net photosynthesis, lower transpiration rate and, thus, higher water use efficiency (Fig. 5D), while *oxr2* mutant plants did not show significant differences with WT plants (Fig. S5B). In addition, the transition to the reproductive phase was delayed in oeOXR2 plants, producing plants with more leaves which flowered approximately four to six days later than WT plants (Fig. S4). All these parameters may explain the increased biomass observed in At*OXR2* overexpressing lines. The main stem diameter was increased, about 40% in average, and oeOXR2 plants also exhibited a higher number of lateral shoots (Fig. 5E), resulting in higher seed production at the end of the life cycle in comparison to WT plants (Fig. 5F).

AtOXR2 modifies the expression of ABA-regulated genes involved in responses to abiotic stress

To evaluate the molecular processes affected by At*OXR2* overexpression, we performed a global transcriptional analysis of 12-leaf rosettes from plants grown under LD photoperiod. We

detected 908 genes differentially regulated with a significance *p*-value below 0.01 and a change in expression level higher than 1.5. Of this group of genes, 473 were upregulated while 441 were downregulated (Table S5A, B). These two sets of genes were used for a set enrichment analysis (SEA) based on GO information (www.geneontology.org). Using the MRCM tool (Fresno *et al.*, 2012), we determined that differentially expressed genes were enriched in Biological Process categories related to "response to stimulus", "stress responses", "programmed cell death" and "lipid transport" (Table S6A), Molecular Function category "catalytic activity" (Table S6B), and Cellular Component category "endomembrane system" (Table S6C).

We also compared the genes differentially expressed in oeOXR2 plants (Table S5) with transcriptional profiles deposited in public databases using Sample Angler (BAR; http://bar.utoronto.ca/ntools/cgi-bin/ntools_sample_angler.cgi). This analysis indicated that the differential expression observed in oeOXR2 plants was similar to that observed in seedlings after ABA treatment for 24 h. The top ten ABA-regulated genes that better correlate between both expression profiles, circled in red in Fig. 6A and listed in Fig. 6B, are related to biotic stress and dehydration responses (Nakabayashi *et al.*, 2005; Goda *et al.*, 2008). We confirmed by RT-qPCR the increased expression of *RAB18*, involved in dehydration stress tolerance (Popova *et al.*, 2015); *TGG2*, coding for a β-thioglucosidase that participates in the defence response mediated by glucosinolates, *CBS*, which codes for an enzyme that regulates chloroplast and mitochondrial redox state (Yoo *et al.*, 2011) and *PDF2.2*, related with the response to fungal pathogens (Stotz *et al.*, 2009) (Fig. 6C). Besides, a significant decrease in the expression of *PDF2.2* was observed in *oxr2.1* mutant plants (Fig. 6C).

Furthermore, we observed a decreased expression of genes linked to ABA synthesis, like *NCED2*, *NCED9* and *AAO4* in oeOXR2 plants (Fig. 6D). NCED9 catalyses the rate-limiting step in ABA synthesis and AAO4 is involved in the last step. We also observed increased levels of transcripts encoding ABA-responsive genes. Among these, we confirmed a higher expression of *ABI5*, involved in ABA signalling during seed maturation and germination (Skubacz *et al.*, 2016), and *TSPO* and *RD29a*, both induced by ABA-mediated stress situations (Guillaumot *et al.*, 2009; Nakashima *et al.*, 2006) (Fig. 6D). These results suggest that oeOXR2 plants have altered ABA metabolism and responses.

Modified At*OXR2* expression generates plants with altered ABA content and responses.

We measured ABA content in seeds and rosette leaves of four-week-old Arabidopsis plants. Increased ABA levels were observed in oeOXR2 plants compared to WT plants in both organs, while no significant changes were evident in the *oxr2.1* mutant (Fig. 7A). This result, the

differential expression of ABA-associated genes (Fig. 6) and the more efficient use of water evidenced in oeOXR2 plants (Fig. 5D), led us to analyse processes related to ABA, like leaf dehydration, stomatal closure, seed germination and seedling establishment (Kang *et al.*, 2015; Hepworth *et al.*, 2016). Detached leaves from oeOXR2 plants showed a significant lower water loss rate, while the *oxr2.1* mutant showed the opposite behaviour in comparison with WT plants (Fig. 7B). Stomatal density was not changed in plants with altered At*OXR2* expression (not shown), suggesting that this not be the cause of differences in water loss. We then analysed stomatal aperture in plants with altered At*OXR2* expression. Rosette-leaves were first incubated in a stomatal opening solution and treated with ABA for 1 h. We quantified the proportion of stomata that were open, mid-open or closed according to a stomatal aperture index (SAI; Eisele *et al.*, 2016). Under control growth conditions, a slight increase in the proportion of closed stomata was evident in oeOXR2 plants (Fig. 7C). After ABA treatment, the proportion of closed stomata was significantly higher in oeOXR2 plants (Fig. 7C), suggesting that these plants have an increased response to ABA. No significant changes were observed in *oxr2.1* mutants (Fig. S6). Based on the known inhibitory effects of ABA on germination, we tested germination and seedling establishment under normal growth conditions and in the presence of different ABA concentrations. While minimal but not significant differences were evident in germination rates (not shown), seedling establishment was less affected by ABA in oeOXR2 plants (Fig. 7D).

AtOXR2 modifies basal ROS levels and oxidative stress tolerance

Given the transcriptomic results and considering that many differentially regulated genes are related to responses to stress (Table S6), we examined ROS content and the behaviour of plants with altered At*OXR2* expression under oxidative stress. Under normal growth conditions, we observed an increase in the intracellular ROS content in 20-day-old oeOXR2 plants, measured by using the cell permeant dye H_2DCFDA (Fig. 8A). This result is also supported by the higher levels of lipid peroxidation measured in oeOXR2 plants at the same stage (Fig. 8B). On the contrary, and in agreement with the phenotypic parameters described above (Fig. 5 and S4), *oxr2* mutants showed no differences with respect to WT plants in the level of ROS content under healthy growing conditions. This could be due to a compensatory or redundant effect exerted by other AtOXR family members that could also be localised into the mitochondria. Next, we evaluated the behaviour of plants with altered levels of AtOXR2 under stress conditions affecting chloroplast and mitochondrial electron transport (Schwarzländer *et al.*, 2009; Cui *et al.*, 2018). We tested the effect of MV and AA, two agents that induce At*OXR2* expression (Fig. 4D), on plant root growth. Under normal growth conditions, roots of oeOXR2 plants were

shorter, while roots of *oxr2* mutants did not exhibit a differential phenotype compared to WT plants (Fig. 8C). Under both stress situations, *oxr2* mutants appeared to be more affected exhibiting shorter roots, while roots of oeOXR2 plants were larger than those of WT plants (Fig. 8D-G). Our results suggest that lack of AtOXR2 can compromise the tolerance to oxidative stress conditions while higher AtOXR2 levels increase the tolerance to agents perturbing the chloroplast and mitochondrial electron transport chain, in agreement with the induction of At*OXR2* by these agents.

Increased expression of At*OXR2* confers tolerance to high-light stress

Among the transcripts differentially expressed in oeOXR2 plants, several were related to secondary metabolism, as well as phenylpropanoid, flavonoid and anthocyanin synthesis (Table S6D). We analysed some of these genes by RT-qPCR in plants with altered expression of At*OXR2* and confirmed a decreased expression of *CHS*, *DFR*, *PAP1* and *UGT79B1*, and an induction of *FLS2* (Fig. S7). This evidence, together with the increased basal ROS levels (Fig. 8A) and the responses to MV and AA (Fig. 8D-G), led us to evaluate the behaviour of oeOXR2 plants under HL intensity (600 µE m^{-2} s^{-1}). We observed a significantly lower decrease caused by HL exposition in several photosynthetic parameters (ΦPSII, Fv/Fm, q_P) in oeOXR2 plants compared to WT plants (Fig. 9A). This result suggests that oeOXR2 plants would be able to convert light into energy (ΦPSII) more efficiently by increasing the q_P and q_N parameters, thus avoiding the potential damage of HL.

Regarding the role of anthocyanins as protective compounds during HL stress, we observed levels comparable to WT in oeOXR2 plants, but lower levels after 3 days of HL exposition (Fig. 9B). This correlates with the lower expression levels of anthocyanin biosynthesis genes in oeOXR2 plants (Table S6D; Fig. S7). In addition, decreased induction of *CHS* and *PAL* were observed after HL stress in oeOXR2 plants (Fig. 9C). These results suggest that the increased tolerance of oeOXR2 plants to HL stress is not related to an increased production of anthocyanins. Another natural compound that could act to ameliorate cellular damage induced by HL stress is ascorbic acid (Foyer and Noctor, 2009; Gallie, 2013; Plumb *et al.*, 2018). Total ascorbate levels were higher in oeOXR2 plants under basal growth conditions (Fig. 9D), suggesting that ascorbic acid may act as a protective compound in oeOXR2 plants.

DISCUSSION

In this work, we showed evidence of a putative role of a single member of the eukaryotic OXR (*OXidation Resistance*) protein family in plants. This family was identified by Volkert and co-workers (2000) during a screening to identify human genes protective against oxidative stress and was later studied in several eukaryotic organisms (Elliott and Volkert, 2004; Durand *et al.*, 2007; Oliver *et al.*, 2011; Wu *et al.*, 2016; Finelli and Oliver, 2017). Using the sequences of OXR1 proteins from yeast and humans (Finelli *et al.*, 2016), we identified four family members in Arabidopsis sharing the canonical ~180 amino acid TLDc domain, characteristic of OXR proteins (Doerks *et al.*, 2002), plus two members, AtOXR4 and AtOXR6, with a truncated TLDc domain (Fig. 1A). Whether AtOXR4 and AtOXR6 represent functional OXR proteins, remains to be determined. In angiosperms, the OXR protein family is represented by five different clades (Fig. 1B). Duplication in embryophytes, probably from OXR4, originated the OXR5 proteins. Later on, a duplication that presumably occurred before the appearance of seed plants produced OXR1 and OXR2, which are more similar to yeast and human OXR1 than members from other clades (Fig. 1B). Proteins of the OXR2 clade are present in gymnosperms and angiosperms (Fig. S1).

The deduced three-dimensional structure of the AtOXR2 TLDc domain matches perfectly with the crystal structure reported for zebrafish DreOXR2 (Blaise *et al.*, 2012) (Fig. 1D). The TLDc domain lacks similarity with other known structures, making difficult the direct association with probable functions. The TLDc domains of proteins from zebrafish and humans do not possess catalase or peroxidase activity but might function by directly reacting with oxidant molecules (Finelli *et al*., 2016; Oliver *et al.*, 2011; Sanada *et al*., 2014; Yang *et al*., 2014). In this sense, Cys-704 of human Oxr1 was proposed as a ROS scavenging amino acid but the oxidation of this residue does not occur in the catalytic range (Oliver *et al*., 2011). This residue, conserved in AtOXR3, is replaced by serine in AtOXR2 (Fig. 1C), probably explaining why AtOXR2 overexpression did not cause a decrease in ROS levels in Arabidopsis, as expected (Fig. 8A, B). The AtOXR2 TLDc domain also contains six cysteines, four of which (Cys-124, 201, 258 and 278) are exposed to the protein surface and therefore probably accessible for redox reactions (Requejo *et al.*, 2010) (Fig. 1C, D). The importance of these residues should be further explored in detail.

AtOXR2 was localised in mitochondria (Fig. 2). Oxr1p from yeast and human Oxr1 are also placed in mitochondria, and this location is essential for protection against oxidative stress induced by H_2O_2 or heat conditions (Elliot and Volkert, 2004; Oliver *et al*., 2011). In this sense, some types of human ALS (Amyotrophic Lateral Sclerosis) originated by respiratory dysfunctions and defects in mitochondrial morphology are alleviated by Oxr1 overexpression (Oliver *et al.*, 2011; Finelli *et al.*, 2015). In agreement, deletion of an Oxr1 isoform present in the

mitochondrial outer membrane (OMM) in mice causes neurodegeneration by de-regulation of phospho-Drp1(Ser616), a key mitochondrial fission regulatory factor (Wu *et al.*, 2016). Concerning AtOXR2, the absence of a canonical cleavable sorting sequence and the predicted structure of β-barrel domains with α-helices in the N-terminal portion suggests a possible OMM localisation (Wiedemann and Pfanner, 2017). OMM localisation was demonstrated for AtVDAC1, AtOM66 and AtPEN2 (Tateda *et al.*,2011; Zhang *et al.*, 2014; Fuchs *et al.*, 2015), three Arabidopsis mitochondrial proteins involved in oxidative stress responses. Further studies using mitochondrial fractionation or fluorescence microscopy techniques (Wagner *et al.*, 2015) will be required to establish the sub-mitochondrial location of AtOXR2. In addition, the presence of AtOXR2 in peroxisomes cannot be excluded, considering that several mitochondrial proteins are also targeted to these organelles (Carrie and Whelan, 2013).

Similarly to Oxr1 and Ncoa7 (Elliot and Volkert 2004; Durand *et al.*, 2007), expression of AtOXR2 targeted to mitochondria alleviates the stress sensitivity of a yeast *oxr1* mutant (Fig. 3). Our results highlight the conserved function of eukaryotic OXR proteins in the protection against oxidative stress. Previous results proposed a role for the *Ipomoea batatas* IbTLD protein in the induction of antioxidant enzymes during wounding stress (Lin *et al.*, 2012).

AtOXR2 overexpression generates plants with a greater number of leaves and increased leaf area, which is associated with an improved photosynthetic performance (Fig. 5, S5). oeOXR2 plants have thicker stems, which may indicate a more efficient transport of photoassimilates from source tissues. All these characteristics translate into increased biomass and seed production (Fig. 5). In sum, oeOXR2 plants exhibit higher capacity to convert the energy contained in the light through photosynthetic fixation of CO_2 into biomass and seed production.. In this sense, there are several reports suggesting that higher expression of functionally different mitochondrial proteins has a positive impact on the generation of plant biomass (Jiang *et al.*, 2014; Racca *et al.*, 2018). Conversely, mutation of At*OXR2* did not produce significant changes in plant biomass or architecture under normal growth conditions. This may reflect the existence of functional redundancy with other mitochondrial family members.

At*OXR2* is expressed broadly and is induced by oxidative stress (Fig. 4). oeOXR2 plants show tolerance to oxidizing conditions imposed by MV or AA and become less affected after exposure to HL (Fig. 8, 9). All these situations impact on the photosynthetic machinery, generating ROS and oxidative damage (Krieger-Liszkay *et al.*, 2011; Niyogi and Truong, 2013; Han *et al.*, 2014). During HL stress, oeOXR2 plants would be able to avoid the damage produced by the excess of excitable energy preventing PSII over-reduction since they contain more ascorbate, which transforms the highly reactive $^1O_2$ into the less harmful molecule H_2O_2 (Kramarenko *et al.*, 2006; Karpinska *et al.*, 2017) (Fig. 9). oeOXR2 plants may also be able to dissipate excess energy by

delivering electrons to another metabolic process or pigments like xanthophyll carotenoids, increasing photochemical and non-photochemical quenching (Ramel *et al.*, 2012; Niyogi and Truong, 2013). Ascorbate promotes plant growth under normal growth conditions and during plant acclimation to HL (Karpinska *et al.*, 2017) and environmental stress (Foyer and Noctor, 2009; Gallie 2013). It is able to divert electrons from the photosynthetic apparatus (Mano *et al*., 2004) and is also required for the conversion of violaxanthin to zeaxanthin, participating in the thermal dissipation of energy under HL (Jahns *et al.*, 2009; Plumb *et al.*, 2018). HL can be a source of stress if it generates photo-damage but can also increase photosynthesis, growth and seed production if plants are naturally resistant or reach acclimation (Triantaphylidès and Havaux, 2009; Athanasiou *et al.*, 2010; Murchie 2017). Cell wall extensibility also depends on ascorbate concentration and the production of ROS in the apoplast (Sharova and Medvedev, 2017), highlighting the key role of ascorbate and its redox state in plant growth and development (Gallie 2013).

Global transcriptional analysis of oeOXR2 plants showed an enrichment of genes related to stress responses, especially those connected to ABA-regulated genes involved in responses to abiotic stress (Fig. 6). Higher expression of At*OXR2* increases ABA levels and modifies ABA metabolism and responses during stomatal closure and seedling establishment (Fig. 7). ABA accumulation promotes changes in gene expression (Shinozaki and Yamaguchi-Shinozaki, 2007), has an impact on root architecture and might contribute to the promotion of cell expansion, stimulating adult plant growth during normal and stress conditions (Humplík *et al*., 2017). Higher ABA levels may contribute to the phenotype of oeOXR2 plants. These plants also have higher ROS levels and there is evidence that the apoplastic accumulation of ROS is involved in the induction of stomatal closure (An *et al*., 2008). Enhanced ROS levels could therefore result in enhanced ABA accumulation, whereas enhanced ABA levels could result in enhanced ROS production in guard cells, thus creating a positive feedback loop (Song *et al.*, 2014).

An interesting question is then how AtOXR2 fulfills its function and alleviates oxidative stress. One possibility is that AtOXR2 directly acts as a ROS scavenger protein, but this seems unlikely in view of the fact that.

Higher expression of At*OXR2* produces an increase in ROS levels under basal growth conditions. ROS can transduce signals as mobile messengers by yet non-elucidated mechanisms (Huang *et al.*, 2016; Vaahtera *et al.*, 2014; Mittler 2017; Mullineaux *et al.*, 2018). H_2O_2, particularly, can originate “priming effects” improving plant performance and promoting cellular proliferation and differentiation (Hossain *et al.*, 2015). ROS are part of retrograde signalling mechanisms from mitochondria or chloroplasts that activate the expression of nuclear-encoded

stress-responsive genes and coordinate the action of phytohormones (Petrov and Van Breusegem, 2012; Bartoli *et al.*, 2013; Crawford *et al.*, 2018). They can also modify the structure and function of target proteins via oxidizing their Cys- residues (Requejo *et al.*, 2010; Akter *et al.*, 2015). These redox-derived changes in protein function can affect transcription, phosphorylation and other important signaling events (Mittler, 2017). In this sense, Finelli and co-workers (2016) demonstrated that TLDc-containing proteins can modulate protein S-nitrosylation in order to protect neurons against oxidative stress.

AtOXR2 may confer tolerance to stress by participating in the systemic acquired acclimation (SAA) network (Mittler and Blumwald, 2015), essential for plant survival to many different stresses. The roles of ROS and ABA in this plant adaptive mechanism were demonstrated (Mittler and Blumwald, 2015). Once AtOXR2 is induced to certain levels during stress, it probably increases the levels of ROS and ABA, setting up the signaling leading to SAA to overcome abiotic stress conditions. The increased ROS levels observed in oeOXR2 plants do not seem to be detrimental for plant growth but may be useful to prime plant acclimation responses. This is suggested by the observed changes in expression of stress- and ABA-related genes. It is tempting to speculate that ROS or modifications in the cellular redox state produced by altering the levels of AtOXR2 induce cellular adaptive responses through changes in gene expression and the activity of hormonal pathways. This question will need further studies to be answered.

SUPPLEMENTARY DATA:

Fig. S1: Phylogenetic tree of OXR2 proteins from different vascular plant species.

Fig. S2: At*OXR2* gene expression map.

Fig. S3: Schematic representation and molecular characterization of the plant lines used in this study.

Fig. S4: Phenotypic analysis of plants with altered At*OXR2* expression.

Fig. S5: Chlorophyll fluorescence parameters measured in oeOXR2 and *oxr2.1* mutant plants during normal growth conditions.

Fig. S6: Stomatal aperture in *oxr2.1* mutant plants.

Fig. S7: Expression analysis of genes involved in the anthocyanin and flavonol biosynthetic pathways in plants with altered expression of At*OXR2*.

Table S1: List of oligonucleotides used in this study.

Table S2: Percent identity matrix of Arabidopsis OXR family members.

Table S3: Sequences used for building the phylogenetic trees.

Table S4: OXR proteins in plants.

Table S5: List of genes up- and downregulated in oeOXR2 plants.

Table S6: GO analysis of terms enriched in the set of genes with modified expression in oeOXR2 plants.

ACKNOWLEDGEMENTS

We are very grateful to Dr. Michael Volkert (University of Massachusetts, USA) for kindly providing us the pMV611 plasmid for yeast complementation assays. We are also very grateful to Dr. Michael Blaise for the excellent comments and help in establishing the homology model of the AtOXR2-TLDc domain. We thank Dr. Marinus Pilon (Colorado State University, Fort Collins, Colorado) for the gift of plastocyanin antibodies. We appreciate the help of Rodrigo Vena and the service provided by the Confocal Microscopy Facility of the Instituto de Biología Molecular y Celular de Rosario (IBR-CONICET-UNR) during the CLSM observations.

FUNDING

This work was supported by grants from CONICET (Consejo Nacional de Investigaciones Científicas y Técnicas. Argentina). ANPCyT (Agencia Nacional de Promoción Científica y Tecnológica. Argentina) and Universidad Nacional del Litoral. DHG, FC, LG and EW are members of CONICET. NM and RM are fellows of the same Institution.

REFERENCES

Akter S, Huang J, Waszczak C, Jacques S, Gevaert K, Van Breusegem F, Messens J. 2015. Cysteines under ROS attack in plants: a proteomics view. Journal of Experimental Botany **66**, 2935–2944.

An Z, Jing W, Liu Y, Zhang W. 2008. Hydrogen peroxide generated by copper amine oxidase is involved in abscisic acid-induced stomatal closure in Vicia faba. Journal of Experimental Botany **59**, 815-825.

Arnold K, Bordoli L, Kopp J, Schwede T. 2006. The SWISS-MODEL workspace: A web-based environment for protein structure homology modelling. Bioinformatics **22**, 195–201.

Athanasiou K, Dyson BC, Webster RE, Johnson GN. 2010. Dynamic Acclimation of Photosynthesis Increases Plant Fitness in Changing Environments. Plant Physiology **152**, 366–373.

Baker NR. 2008. Chlorophyll Fluorescence: A Probe of Photosynthesis In Vivo. Annual Review

of Plant Biology **59**, 89–113.

Bartoli CG, Casalongué CA, Simontacchi M, Marquez-Garcia B, Foyer CH. 2013. Interactions between hormone and redox signalling pathways in the control of growth and cross tolerance to stress. Environmental and Experimental Botany **94**, 73–88.

Blaise M, Alsarraf H, Wong J, *et al*. 2012. Crystal structure of the TLDc domain of oxidation resistance protein 2 from zebrafish. Proteins: Structure, Function and Bioinformatics **80**, 1694–1698.

Boratyn GM, Camacho C, Cooper PS, *et al.* 2013. BLAST: a more efficient report with usability improvements. Nucleic Acids Research **41**, W29-33.

Boyes DC, Zayed AM, Ascenzi R, *et al*. 2001. Growth Stage – Based Phenotypic Analysis of Arabidopsis: A Model for High Throughput Functional Genomics in Plants. The Plant Cell **13**, 1499–1510.

Brady SM, Orlando DA, Lee JY, *et al.* (2007) A High-Resolution Root Spatiotemporal Map Reveals Dominant Expression Patterns. Science **318**, 801–806.

Campeau PM, Hennekam RC, Aftimos S, *et al.* 2014. DOORS syndrome: Phenotype, genotype and comparison with coffin-siris syndrome. American Journal of Medical Genetics, Part C: Seminars in Medical Genetics **166**, 327–332.

Carrie C, Whelan J. 2013. Widespread dual targeting of proteins in land plants: When, where, how and why. Plant Signaling & Behavior **8**, e25034.

Clough SJ, Bent AF. 1998. Floral dip: A simplified method for Agrobacterium-mediated transformation of Arabidopsis thaliana. The Plant Journal **16**, 735–743.

Crawford T, Lehotai N, Strand Å. 2018. The role of retrograde signals during plant stress responses. Journal of Experimental Botany **69**, 2783–2795.

Cui F, Brosche M, Shapiguzov A, He XQ, Vainonen J, *et al*. 2018. Methyl viologen can affect mitochondrial function in Arabidopsis. bioRxiv, **436543**.

Cvetkovska M, Alber NA, Vanlerberghe GC. 2012. The signaling role of a mitochondrial superoxide burst during stress. Plant signaling & behavior **8**, e22749.

Czarnocka W, Karpiński S. 2018. Friend or foe? Reactive oxygen species production, scavenging and signaling in plant response to environmental stresses. Free Radical Biology and

Medicine **122,** 4-20.

Czechowski T. 2005. Genome-Wide Identification and Testing of Superior Reference Genes for Transcript Normalization in Arabidopsis. Plant Physiology **139**, 5–17.

Delport W, Poon AFY, Frost SDW, *et al*. 2010. Datamonkey 2010: A suite of phylogenetic analysis tools for evolutionary biology. Bioinformatics **26**, 2455–2457.

Dietz K-J, Mittler R, Noctor G. 2016. Recent Progress in Understanding the Role of Reactive Oxygen Species in Plant Cell Signaling. Plant Physiology **171**, 1535–1539.

Doerks T, Copley RR, Schultz J, Ponting CP, Bork P. 2002. Systematic identification of novel protein domain families associated with nuclear functions. Genome Research **12**, 47–56.

Durand M, Kolpak A, Farrell T, *et al*. 2007. The OXR domain defines a conserved family of eukaryotic oxidation resistance proteins. BMC Cell Biology **8**, 13.

Durgbanshi A, Arbona V, Pozo O, Miersch O, Sancho J V, Gómez-Cadenas A. 2005. Simultaneous determination of multiple phytohormones in plant extracts by liquid chromatography-electrospray tandem mass spectrometry. Journal of Agricultural and Food Chemistry **53**, 8437–8442.

Earley KW, Haag JR, Pontes O, Opper K, Juehne T, Song K, Pikaard CS. 2006. Gateway-compatible vectors for plant functional genomics and proteomics. The Plant Journal **45**, 616–629.

Edgar R. 2002. Gene Expression Omnibus: NCBI gene expression and hybridization array data repository. Nucleic Acids Research **30**, 207-210.

Eisele JF, Fäßler F, Bürgel PF, Chaban C. 2016. A rapid and simple method for microscopy-based stomata analyses. PLoS ONE **11:** e0164576. .

Elliott N a, Volkert MR. 2004. Stress induction and mitochondrial localization of Oxr1 proteins in yeast and humans. Molecular and cellular biology **24**, 3180–3187.

El-Gebali S, Mistry J, Bateman A, Eddy SR, *et al*. 2019. The Pfam protein families database in 2019. Nucleic Acids Research **8,** D427-D432.

Fankhauser N, Mäser P. 2005. Identification of GPI anchor attachment signals by a Kohonen self-organizing map. Bioinformatics **21**, 1846–1852.

Finelli MJ, Liu KX, Wu Y, Oliver PL, Davies KE. 2015. Oxr1 improves pathogenic cellular features of ALS-associated FUS and TDP-43 mutations. Human Molecular Genetics **24**, 3529–3544.

Finelli MJ, Oliver PL. 2017. TLDc proteins: new players in the oxidative stress response and neurological disease. Mammalian Genome **28**, 395–406.

Finelli MJ, Sanchez-Pulido L, Liu KX, Davies KE, Oliver PL. 2016. The evolutionarily conserved Tre2/Bub2/Cdc16 (TBC), lysin motif (LysM), domain catalytic (TLDc) domain is neuroprotective against oxidative stress. Journal of Biological Chemistry **291**, 2751–2763.

Fischer H, Zhang XU, O'Brien KP, Kylsten P, Engvall E. 2001. C7, a novel nucleolar protein, is the mouse homologue of the Drosophila late puff product l82 and an isoform of human OXR1. Biochemical and Biophysical Research Communications **281**, 795–803.

Foyer C, Noctor G. 2009. Redox regulation in photosynthetic organisms: signaling, acclimation, and practical implications. Antioxidants & redox signaling **11**, 861-905.

Foyer CH, Noctor G. 2016. Stress-triggered redox signalling: What's in pROSpect? Plant Cell and Environment **39**, 951–964.

Foyer CH, Ruban A V, Noctor G. 2017. Viewing oxidative stress through the lens of oxidative signalling rather than damage. Biochemical Journal **474,** 877-883.

Fresno C, Llera AS, Girotti MR, *et al*. 2012. The multi-reference contrast method: Facilitating set enrichment analysis. Computers in Biology and Medicine **42**, 188–194.

Fuchs R, Kopischke M, Klapprodt C, *et al*. 2015. Immobilized subpopulations of leaf epidermal mitochondria mediate PEN2-dependent pathogen entry control in Arabidopsis. The Plant Cell **28,** 130-145.

Fukasawa Y, Tsuji J, Fu S-C, *et al*. 2015. MitoFates: Improved Prediction of Mitochondrial Targeting Sequences and Their Cleavage Sites. Molecular & Cellular Proteomics **14**, 1113–1126.

Gallie DR. 2013. The role of l-ascorbic acid recycling in responding to environmental stress and in promoting plant growth. Journal of Experimental Botany **64**, 433–443.

Gentleman R, Carey V, Bates D, *et al.* 2004. Bioconductor: open software development for computational biology and bioinformatics. Genome Biology **5**, R80.

Gillespie KM, Ainsworth EA. 2007. Measurement of reduced, oxidized and total ascorbate content in plants. Nature Protocols **2**, 871–874.

Gleason C, Huang S, Thatcher LF, *et al*. 2011. Mitochondrial complex II has a key role in mitochondrial-derived reactive oxygen species influence on plant stress gene regulation and defense. Proceedings of the National Academy of Sciences of the United States of America **108**, 10768–73.

Goda H, Sasaki E, Akiyama K, *et al.* 2008. The AtGenExpress hormone and chemical treatment data set: Experimental design, data evaluation, model data analysis and data access. The Plant Journal **55**, 526–542.

Goodstein DM, Shu S, Howson R, *et al.* 2012. Phytozome: A comparative platform for green plant genomics. Nucleic Acids Research **40,** D1178-D1186.

Gouy M, Guindon S, Gascuel O. 2010. SeaView Version 4: A Multiplatform Graphical User Interface for Sequence Alignment and Phylogenetic Tree Building. Molecular Biology and Evolution **27**, 221–224.

Guillaumot D, Guillon S, Déplanque T, *et al*. 2009. The Arabidopsis TSPO-related protein is a stress and abscisic acid-regulated, endoplasmic reticulum-Golgi-localized membrane protein. Plant Journal **60,** 242-256.

Han HJ, Peng RH, Zhu B, *et al*. 2014. Gene expression profiles of arabidopsis under the stress of methyl viologen: a microarray analysis. Molecular Biology Reports **41**, 7089–7102.

Hepworth C, Turner C, Landim MG, Cameron D, Gray JE. 2016. Balancing water uptake and loss through the coordinated regulation of stomatal and root development. PLoS ONE **11:** e0156930.

Hodges DM, DeLong JM, Forney CF, Prange RK. 1999. Improving the thiobarbituric acid-reactive-substances assay for estimating lipid peroxidation in plant tissues containing anthocyanin and other interfering compounds. Planta **207,** 604–611.

Hooper CM, Castleden IR, Tanz SK, Aryamanesh N, Millar AH. 2017. SUBA4: The interactive data analysis centre for Arabidopsis subcellular protein locations. Nucleic Acids Research **45**, D1064–D1074.

Hossain MA, Bhattacharjee S, Armin S-M, Qian P, Xin W, Li H-Y, Burritt DJ, Fujita M, Tran L-SP. 2015. Hydrogen peroxide priming modulates abiotic oxidative stress tolerance:

insights from ROS detoxification and scavenging. Frontiers in Plant Science **6**.

Humplík JF, Bergougnoux V, Van Volkenburgh E. 2017. To Stimulate or Inhibit? That Is the Question for the Function of Abscisic Acid. Trends in Plant Science **22**, 830–841.

Jahns P, Latowski D, Strzalka K. 2009. Mechanism and regulation of the violaxanthin cycle: The role of antenna proteins and membrane lipids. Biochimica et Biophysica Acta - Bioenergetics **1787**, 3–14.

Jaramillo-Gutierrez G, Molina-Cruz A, Kumar S, Barillas-Mury C. 2010. The Anopheles gambiae oxidation resistance 1 (OXR1) gene regulates expression of enzymes that detoxify reactive oxygen species. PLoS ONE **5**, 1–9.

Jardim-Messeder D, Caverzan A, Rauber R, *et al*. 2015. Succinate dehydrogenase (mitochondrial complex II) is a source of reactive oxygen species in plants and regulates development and stress responses. New Phytologist **208,** 776-789.

Jefferson RA, Kavanagh TA, Bevan MW. 1987. GUS fusions: beta-glucuronidase as a sensitive and versatile gene fusion marker in higher plants. The EMBO journal **6**, 3901–7.

Jiang C, Tholen D, Xu JM, *et al*. 2014. Increased expression of mitochondria-localized carbonic anhydrase activity resulted in an increased biomass accumulation in Arabidopsis thaliana. Journal of Plant Biology **57**, 366–374.

Kang J, Yim S, Choi H, *et al*. 2015. Abscisic acid transporters cooperate to control seed germination. Nature Communications **6**.

Karpinska B, Zhang K, Rasool B, *et al.* 2017. The redox state of the apoplast influences the acclimation of photosynthesis and leaf metabolism to changing irradiance. Plant Cell and Environment **41,**1083-1097.

Kiefer F, Arnold K, Künzli M, Bordoli L, Schwede T. 2009. The SWISS-MODEL Repository and associated resources. Nucleic Acids Research **37**.

Kobayashi N, Takahashi M, Kihara S, *et al*. 2014. Cloning of cDNA encoding a Bombyx mori homolog of human oxidation resistance 1 (OXR1) protein from diapause eggs, and analyses of its expression and function. Journal of Insect Physiology **68**, 58–68.

Kramarenko GG, Hummel SG, Martin SM, Buettner GR. 2006. Ascorbate Reacts with Singlet Oxygen to Produce Hydrogen Peroxide. Photochemistry and Photobiology **82**, 1634.

Krieger-Liszkay A, Kós PB, Hideg É. 2011. Superoxide anion radicals generated by methylviologen in photosystem I damage photosystem II. Physiologia Plantarum **142**, 17–25.

Laroche FJF, Tulotta C, Lamers GEM, Meijer AH, Yang P, Verbeek FJ, Blaise M, Stougaard J, Spaink HP. 2013. The embryonic expression patterns of zebrafish genes encoding LysM-domains. Gene Expression Patterns **13**, 212–224.

Lee J, Durst RW, Wrolstad RE. 2005. Determination of total monomeric anthocyanin pigment content of fruit juices, beverages, natural colorants, and wines by the pH differential method: Collaborative study. Journal of AOAC International **88**, 1269–1278.

Letunic I, Bork P. 2016. Interactive tree of life (iTOL) v3: an online tool for the display and annotation of phylogenetic and other trees. Nucleic Acids Research **44**, W242–W245.

Liebthal M, Maynard D, Dietz K-J. 2017. Peroxiredoxins and Redox Signaling in Plants. Antioxidants & Redox Signaling, ars.2017.7164.

Lin JS, Lin CC, Lin HH, Chen YC, Jeng ST. 2012. MicroR828 regulates lignin and h2O2 accumulation in sweet potato on wounding. New Phytologist **196,** 427-40.

Liu KX, Edwards B, Lee S, *et al*. 2015. Neuron-specific antioxidant OXR1 extends survival of a mouse model of amyotrophic lateral sclerosis. Brain: A journal of neurology **138**, 1167–81.

Logan DC, Leaver CJ. 2000. Mitochondria-targeted GFP highlights the heterogeneity of mitochondrial shape, size and movement within living plant cells. Journal of Experimental Botany **51**, 865–871.

Löytynoja A, Goldman N. 2010. WebPRANK: A phylogeny-aware multiple sequence aligner with interactive alignment browser. BMC Bioinformatics **11,** 579.

Maki M, Kitaura Y, Satoh H, Ohkouchi S, Shibata H. 2002. Structures, functions and molecular evolution of the penta-EF-hand Ca2+-binding proteins. Biochimica et biophysica acta **1600**, 51–60.

Mano J, Hideg É, Asada K. 2004. Ascorbate in thylakoid lumen functions as an alternative electron donor to photosystem II and photosystem I. Archives of Biochemistry and Biophysics **429**, 71–80.

Maxwell K, Johnson GN. 2000. Chlorophyll fluorescence—a practical guide. Journal of Experimental Botany **51**, 659–668.

Mittler R. 2017. ROS Are Good. Trends in Plant Science **22**, 11–19.

Mittler R, Blumwald E. 2015. The Roles of ROS and ABA in Systemic Acquired Acclimation. The Plant Cell **27**, 64–70.

Mittler R, Vanderauwera S, Suzuki N, *et al*. 2011. ROS signaling: The new wave? Trends in Plant Science **16**, 300–309.

Moreno-Piovano GS, Moreno JE, Cabello JV, *et al*. 2017. A role for LAX2 in regulating xylem development and lateral-vein symmetry in the leaf. Annals of Botany **120**, 577–590.

Mullineaux PM, Exposito-Rodriguez M, Laissue PP, Smirnoff N. 2018. ROS-dependent signalling pathways in plants and algae exposed to high light: Comparisons with other eukaryotes. Free Radical Biology and Medicine **122**, 52-64.

Murchie EH. 2017. Safety conscious or living dangerously: what is the 'right' level of plant photoprotection for fitness and productivity? Plant Cell and Environment **40**, 1239–1242.

Nakabayashi K, Okamoto M, Koshiba T, Kamiya Y, Nambara E. 2005. Genome-wide profiling of stored mRNA in Arabidopsis thaliana seed germination: Epigenetic and genetic regulation of transcription in seed. The Plant Journal **41**, 697–709.

Nakagawa T, Suzuki T, Murata S, *et al.* 2007. Improved Gateway Binary Vectors: High-Performance Vectors for Creation of Fusion Constructs in Transgenic Analysis of Plants. Bioscience, Biotechnology, and Biochemistry **71**, 2095–2100.

Nakashima K, Fujita Y, Katsura K, *et al*. 2006. Transcriptional Regulation of ABI3- and ABA-responsive Genes Including RD29B and RD29A in Seeds, Germinating Embryos, and Seedlings of Arabidopsis. Plant Molecular Biology **60**, 51–68.

Natoli R, Provis J, Valter K, Stone J. 2008. Expression and role of the early-response gene Oxr1 in the hyperoxia-challenged mouse retina. Investigative Ophthalmology and Visual Science **49**, 4561–4567.

Navrot N, Rouhier N, Gelhaye E, Jacquot JP. 2007. Reactive oxygen species generation and antioxidant systems in plant mitochondria. Physiologia Plantarum **129**, 185–195.

Nelson BK, Cai X, Nebenführ A. 2007. A multicolored set of in vivo organelle markers for co-localization studies in Arabidopsis and other plants. The Plant Journal **51**, 1126–1136.

Niyogi KK, Truong TB. 2013. Evolution of flexible non-photochemical quenching mechanisms

that regulate light harvesting in oxygenic photosynthesis. Current Opinion in Plant Biology **16**, 307–314.

Noctor G, Reichheld JP, Foyer CH. 2017. ROS-related redox regulation and signaling in plants. Seminars in Cell and Developmental Biology **80**, 3-12.

O'Connell J. 2002. The Basics of RT-PCR. Methods in Molecular Biology, vol. 193: RT-PCR Protocols Edited by:J. O'Connell © Humana Press Inc., Totowa, NJ, 19–25.

Oliver PL, Finelli MJ, Edwards B, *et al*. 2011. Oxr1 is essential for protection against oxidative stress-induced neurodegeneration. PLoS Genetics **7**, e1002338.

Plumb W, Townsend AJ, Rasool B, *et al*. 2018. Ascorbate-mediated regulation of growth, photoprotection and photoinhibition in Arabidopsis thaliana. Journal of Experimental Botany **69,** 2823-2835.

Popova A., Rausch S, Hundertmark M, Gibon Y, Hincha DK. 2015. The intrinsically disordered protein LEA7 from Arabidopsis thaliana protects the isolated enzyme lactate dehydrogenase and enzymes in a soluble leaf proteome during freezing and drying. Biochimica et biophysica acta **1854**, 1517–1525.

R Development Core Team. 2014. R: A language and environment for statistical computing. R Foundation for Statistical Computing, Vienna, Austria. URL http://www.R-project.org/.

Racca S, Welchen E, Gras DE, *et al*. 2018. Interplay between cytochrome c and gibberellins during Arabidopsis vegetative development. The Plant Journal **94,** 105-121.

Ramel F, Birtic S, Ginies C, *et al*. 2012. Carotenoid oxidation products are stress signals that mediate gene responses to singlet oxygen in plants. Proceedings of the National Academy of Sciences **109**, 5535–5540.

Requejo R, Hurd TR, Costa NJ, Murphy MP. 2010. Cysteine residues exposed on protein surfaces are the dominant intramitochondrial thiol and may protect against oxidative damage. FEBS Journal **6,** 1465-1480.

Robinson SJ, Tang LH, Mooney BA, *et al.* 2009. An archived activation tagged population of Arabidopsis thaliana to facilitate forward genetics approaches. BMC Plant Biology **9,** 101.

Samson F, Brunaud V, Balzergue S, Dubreucq B, Lepiniec L, Pelletier G, Caboche M, Lecharny a. 2002. FLAGdb/FST: a database of mapped flanking insertion sites (FSTs) of

Arabidopsis thaliana T-DNA transformants. Nucleic Acids Research **30**, 94–97.

Sanada Y, Asai S, Ikemoto A, Moriwaki T, Nakamura N, Miyaji M, Zhang-Akiyama Q-M. 2014. Oxidation resistance 1 (OXR1) is essential for protection against oxidative stress and participates in the regulation of aging in Caenorhabditis elegans. Free radical research **1**, 1–27.

Schindelin J, Arganda-Carreras I, Frise E, *et al.* 2012. Fiji: An open-source platform for biological-image analysis. Nature Methods **9**, 676–682.

Schwacke R, Schneider A, van der Graaff E, Fischer K, Catoni E, Desimone M, Frommer WB, Flügge U-I, Kunze R. 2003. ARAMEMNON, a novel database for Arabidopsis integral membrane proteins. Plant physiology **131**, 16–26.

Schwarzländer M, König AC, Sweetlove LJ, Finkemeier I. 2012. The impact of impaired mitochondrial function on retrograde signalling: a meta-analysis of transcriptomic responses. Journal of Experimental Botany **63**, 1735–1750.

Sharova EI, Medvedev SS. 2017. Redox reactions in apoplast of growing cells. Russian Journal of Plant Physiology **64**, 1–14.

Shinozaki K, Yamaguchi-Shinozaki K. 2007. Gene networks involved in drought stress response and tolerance. Journal of Experimental Botany **58,** 221–227.

Shkolnik K, Ben-Dor S, Galiani D, Hourvitz A, Dekel N. 2008. Molecular characterization and bioinformatics analysis of Ncoa7B, a novel ovulation-associated and reproduction system-specific Ncoa7 isoform. Reproduction **135**, 321–333.

Sievers F, Wilm A, Dineen D, *et al.* 2014. Fast, scalable generation of high-quality protein multiple sequence alignments using Clustal Omega. Molecular Systems Biology **7**, 539–539.

Silver JD, Ritchie ME, Smyth GK. 2009. Microarray background correction: Maximum likelihood estimation for the normal-exponential convolution. Biostatistics **10**, 352–363.

Skubacz A, Daszkowska-Golec A, Szarejko I. 2016. The role and regulation of *ABI5* (*ABA-Insensitive 5*) in plant development, abiotic stress responses and phytohormone crosstalk. Frontiers in Plant Science **7,** 1884.

Song Y, Miao Y, Song CP. 2014. Behind the scenes: The roles of reactive oxygen species in guard cells. New Phytologist **201**, 1121–1140.

Steinebrunner I, Landschreiber M, Krause-Buchholz U, Teichmann J, Rodel G. 2011.

HCC1, the Arabidopsis homologue of the yeast mitochondrial copper chaperone SCO1, is essential for embryonic development. Journal of Experimental Botany **62**, 319–330.

Stowers RS, Russell S, Garza D. 1999. The 82F late puff contains the L82 gene, an essential member of a novel gene family. Developmental biology **213**, 116–30.

Su L-D De, Zhang Q-LL, Lu Z. 2017. Oxidation resistance 1 (OXR1) participates in silkworm defense against bacterial infection through the JNK pathway. Insect Science **24**, 17–26.

Tateda C, Watanabe K, Kusano T, Takahashi Y. 2011. Molecular and genetic characterization of the gene family encoding the voltage-dependent anion channel in Arabidopsis. Journal of Experimental Botany **62**, 4773–4785.

Triantaphylidès C, Havaux M. 2009. Singlet oxygen in plants: production, detoxification and signaling. Trends in Plant Science **14**, 219–228.

Vaahtera L, Brosché M, Wrzaczek M, Kangasjärvi J. 2014. Specificity in ROS Signaling and Transcript Signatures. Antioxidants & Redox Signaling **21**, 1422–1441.

Van Breusegem F, Bailey-Serres J, Mittler R. 2008. Unraveling the Tapestry of Networks Involving Reactive Oxygen Species in Plants. Plant Physiology **147**, 978–984.

Vanlerberghe GC. 2013. Alternative oxidase: A mitochondrial respiratory pathway to maintain metabolic and signaling homeostasis during abiotic and biotic stress in plants. International Journal of Molecular Sciences **14**, 6805–6847.

Vercesi AE, Borecký J, Maia I de G, Arruda P, Cuccovia IM, Chaimovich H. 2006. Plant uncoupling mitochondrial proteins. Annual Review of Plant Biology **57**, 383–404.

Volkert MR, Elliott NA, Housman DE. 2000. Functional genomics reveals a family of eukaryotic oxidation protection genes. Proceedings of the National Academy of Sciences of the United States of America **97**, 14530–14535.

Waese J, Fan J, Pasha A, *et al.* 2017. ePlant: Visualizing and Exploring Multiple Levels of Data for Hypothesis Generation in Plant Biology. The Plant Cell **29**, 1806-1821

Wagner S, Behera S, De Bortoli S, *et al.* 2015. The EF-Hand Ca2+ Binding Protein MICU Choreographs Mitochondrial Ca2+ Dynamics in Arabidopsis. The Plant Cell **27**, 3190–212.

Wang Z, Berkey CD, Watnick PI. 2012. The Drosophila protein mustard tailors the innate immune response activated by the immune deficiency pathway. Journal of immunology **188**,

3993–4000.

Wang Z, Hang S, Purdy AE, Watnick PI. 2013. Mutations in the IMD pathway and mustard counter Vibrio cholerae suppression of intestinal stem cell division in Drosophila. mBio **4**, 1–9.

Wang J, Sarker AH, Cooper PK, Volkert MR. 2004. The Single-Strand DNA Binding Activity of Human PC4 Prevents Mutagenesis and Killing by Oxidative DNA Damage The Single-Strand DNA Binding Activity of Human PC4 Prevents Mutagenesis and Killing by Oxidative DNA Damage **24**, 6084–6093.

Wiedemann N, Pfanner N. 2017. Mitochondrial Machineries for Protein Import and Assembly. Annual Review of Biochemistry **86**, 685–714.

Wu Y, Davies KE, Oliver PL. 2016. The antioxidant protein Oxr1 influences aspects of mitochondrial morphology. Free Radical Biology and Medicine **95**, 255–267.

Yang M, Luna L, Sørbø JG, *et al*. 2014. Human OXR1 maintains mitochondrial DNA integrity and counteracts hydrogen peroxide-induced oxidative stress by regulating antioxidant pathways involving p21. Free Radical Biology and Medicine **77**, 41–48.

Yoo KS, Ok SH, Jeong B-C, *et al*. Single Cystathionine -Synthase Domain-Containing Proteins Modulate Development by Regulating the Thioredoxin System in Arabidopsis. The Plant Cell **23**, 3577–3594.

Zhang B, Van Aken O, Thatcher L, *et al.* 2014. The mitochondrial outer membrane AAA ATPase AtOM66 affects cell death and pathogen resistance in Arabidopsis thaliana. The Plant Journal **80**, 709–727.

FIGURE LEGENDS

Figure 1: The Oxidation Resistance protein family in plants. (A) Schematic representation of domain architecture of the six members of the Arabidopsis AtOXR protein family (AtOXR1, NP_195697.3; AtOXR2, NP_849938.1; AtOXR3, NP_196244.1; AtOXR4, NP_174530.2; AtOXR5, NP_198775.1; AtOXR6, NP_195133.3), together with OXR1 proteins from yeast (*S. cerevisiae*, ScOXR1, NP_015128.1) and humans (HsOXR1, NP_001185464.1), used for the identification of Arabidopsis members. The gene identification code (GI) corresponds to the AGI (Arabidopsis Genome Initiative) number for Arabidopsis, the Saccharomyces systematic name and the HGNC (HUGO Gene Nomenclature Committee) number for human OXR1. For AtOXR3 and AtOXR6, the EFh domains are shown. For human OXR1, a LysM (Lysin Motif) and GRAM protein domains are drawn. (**B)** Phylogenetic tree of OXR proteins from selected plant species. An alignment of TLDc-containing protein sequences from 18 members of the *Viridiplantae* was used to construct a phylogenetic tree. Different clades are represented by different colors. OXR1 from *S. cerevsiae* and *H. sapiens* were included. See Table S3 for detailed information about the sequence of the proteins used during this analysis. **(C)** Sequence alignment of the TLDc domain region of AtOXR2 (NP_849938.1), human (HsOXR1, NP_001185461), zebrafish (DreOXR2, NP_001107916.1), Drosophila (DmOXR1, NP_730913.1) and yeast (ScOXR1, NP_015128.1) eukaryotic OXR family members. Conserved glycine (Gly-93, Gly-174) and glutamic acid (Glu-216) residues are marked with arrowheads. Cys-704 of human OXR1, proposed to be involved in ROS scavenging, is indicated by a black arrow. The four exposed cysteines in AtOXR2 (Cys-124, 201, 258 and 278) are marked with asterisks. The alignment was created using the MView tool of CLUSTAL OMEGA (https://www.ebi.ac.uk/Tools/msa/clustalo/). **(D)** Structure of the AtOXR2 TLDc domain based on the DreOXR2 crystal structure (Blaise *et al.*, 2012). The structure consists of a β-sandwich surrounded by two helices and two one-turn helices. The four α-helices and ten β-strands are shown in rose and yellow, respectively.

Figure 2: AtOXR2 is localised in mitochondria. (A) Seedlings of 15-day-old transgenic lines co-expressing AtOXR2-mRFP and mito-GFP were imaged by CLSM. Representative cells from roots (a-c) and leaves (d-i) are shown, in which the signals for AtOXR2-mRFP (magenta; panels a and d) and mito-GFP (green; panels b and e) co-localise as merged white dot-signals (c, f). Chlorophyll fluorescence of chloroplasts is observed in cyan in panels g-i. No co-localisation of the AtOXR2-mRFP signals with chloroplasts was observed. A bright field image is shown in i. **(B)** Subcellular localisation analysis of AtOXR2 by Western blot. Mitochondria enriched

extracts (M) and fractions I and II (F I-II; see Materials and methods for details) from fully expanded 20-day-old rosette leaves of a representative transgenic line expressing 35S:AtOXR2-GFP and WT plants were loaded in a 15% SDS-PAGE and transferred to a PVDF membrane. Blots were analysed with antibodies against GFP (abcam #ab290; for the fusion protein AtOXR2-GFP), COX2 (mitochondrial marker), plastocyanin (PC; chloroplast marker) and actin (cytosol marker). A Ponceau-staining of the membrane, with a prominent protein band probably corresponding to the large subunit of Rubisco, is shown.

Figure 3: **AtOXR2 expression protects yeast cells from oxidative damage.** An *oxr1* yeast mutant strain was transformed with a construct expressing AtOXR2 fused to the MTS of yeast Sod2p in its N-terminal portion, and under the control of a constitutive yeast promoter (*oxr1*/AtOXR2) or with the empty vector (*oxr1*). Cells were grown in standard YEPD medium and treated with 100 or 150 µM H_2O_2 during 1 h at 30°C. Serial dilutions of the cultures at OD_{600} of approximately 0.8-1 were applied to plates containing YEPD medium and incubated at 30ºC for 2 days. BY4742 is the WT strain from which the *oxr1* mutant was obtained.

Figure 4: Expression profile of the At*OXR2* gene. (A) Histochemical analysis of *GUS* reporter gene expression driven by the At*OXR2* promoter. Strong expression was observed in trichomes of nascent leaves (a-c, e), in cotyledon tips and veins (b), and in the apical meristem and leaf primordia (b, c). Expression was also observed in vascular tissues of hypocotyls, leaves and roots (d, h) and in mature pollen grains (compare f and g). **(B)** GUS activity levels measured in protein extracts from 2-week-old Arabidopsis seedlings and in rosette leaves, roots, fully opened flowers and siliques from adult plants. **(C)** GUS activity levels measured in protein extracts from mature rosette leaves of plants grown under normal conditions (Control) or exposed to HL (600 µmol m^{-2} s^{-1}, 6 h), UV-B (30 min exposure followed by a 3-h recovery period) or 3-AT (4 mM, 3 h). **(D)** At*OXR2* transcript levels measured in Arabidopsis WT seedlings grown for 7 DAS in 0.5 x MS medium and then transfer to a solution containing MS (MS, control) or the same medium supplemented with 0.1 µM MV for 3 h, 10 µM AA for 6 h, or exposed to UV-B (5 mW/cm^2; UVP 34-0042-01 lamp) for 1 h. Experiments were carried out with approximately 50 plants per biological replicate. Results are expressed as mean±SEM of three independent experiments. Asterisks represent significantly different values at $P < 0.05$ (ANOVA; Tukey test).

Figure 5: Phenotypic analysis and photosynthetic parameters of oeOXR2 and *oxr2* mutant plants. (A) Representative image of rosettes from plants grown in LD photoperiod during 32 DAS (see Fig. S4 for details). **(B)** Parameters related to rosette growth: rosette area and number of leaves in WT, oeOXR2 and *oxr2.2* plants at different DAS. **(C)** ETR measured at different light intensities (from 0 to 2000 µmol m^{-2} s^{-1}) in fully expanded rosette leaves of WT and oeOXR2 plants at 32 DAS. **(D)** Net photosynthesis, transpiration rate and water use efficiency in WT and oeOXR2 plants. Measurements were made in the 6^{th} leaf pair of plants at the same developmental stage. **(E)** Stem diameter and secondary shoots at the end of the life cycle for oeOXR2 and *oxr2.2* plants. **(F)** Seed production, expressed as mg of seeds per plant, was obtained by weighing seeds from ten individual plants. Values represent the mean±SD. Asterisks indicate significant differences ($P < 0.01$) with WT plants according to LSD Fisher tests. Two independent oeOXR2 lines, named oeOXR2 A and B, were used.

Figure 6: Genes related with ABA metabolism and responses show altered expression in oeOXR2 plants. (A) Scatter plot comparing the expression of genes induced in WT seeds incubated with ABA for 24 h during germination and those induced in oeOXR2 plants (see Table S5B). **(B)** List of the 10 best scoring ABA-induced genes with induced expression in oeOXR2 plants, according to the Sample angler tool (r-value cutoff: 0.75). **(C)** Analysis of gene expression by RT-qPCR of four genes (*RAB18*, *TGG2*, *PDF2.2* and *CBS*) from the list in (B). (**D)** Expression analysis by RT-qPCR of ABA biosynthetic pathway and ABA-responsive genes (*NCED2* and *9*, *NINE-CIS-EPOXYCAROTENOID DIOXYGENASE 2* and *9*; *AAO4*, *ALDEHYDE OXIDASE 4*; *ABI5*, *ABA INSENSITIVE* 5; *RD29a*, *RESPONSIVE TO DESICCATION 29a* and *TSPO*, *OUTER MEMBRANE TRYPTOPHAN-RICH SENSORY PROTEIN*) that were down or upregulated in the transcriptomic analysis of oeOXR2 plants. Expression analysis was performed on 12-leaf rosettes of plants overexpressing At*OXR2* (two independent lines, A and B, *oxr2.2* mutants, and WT plants. Results are expressed as mean±SD of biological triplicates containing pools of approximately 20 individual plants each. Asterisks represent significantly different values at $P < 0.05$ (t-test or ANOVA; Tukey test for multiple comparisons).

Figure 7: At*OXR2* overexpression generates plants with higher ABA content and altered ABA responses. (A) ABA content in seeds and in four-week-old Arabidopsis rosette leaves of oeOXR2 plants, *oxr2.1* mutants, and the corresponding WT plants. **(B)** Water loss between 0 and 210 min in fully developed detached leaves. **(C)** Stomatal aperture in oeOXR2 A and B lines was quantified under normal growth conditions (control), after incubation in the opening solution

(Open Sol., see Materials and methods), and in the presence of ABA for 1 h. Image analysis was performed using Fiji software. The stomatal aperture index (SAI) was calculated as the ratio of stomatal length to width. **(D)** Differences in seedling establishment between oeOXR2 and WT plants in MS 0.5x and in the presence of 4 µM ABA. Results are expressed as mean±SD of sixty plants for each genotype. Asterisks represent significantly different values at $P < 0.05$ (t-test or ANOVA; Tukey test for multiple comparisons).

Figure 8: AtOXR2 modifies basal ROS levels and oxidative stress tolerance. (A) Intracellular ROS content in Arabidopsis rosette leaves of oeOXR2, *oxr2.2* and WT plants, quantified by the level of fluorescence using the cell permeant dye H_2DCFDA. **(B)** Lipid peroxidation expressed as nmol of thiobarbituric acid reactive substances (TBARS) per mg of tissue (fresh weight). Both parameters (**A, B**) were measured in fully expanded rosette leaves of 20-day-old plants grown under normal conditions. **(C)** Primary root length measured in seedlings vertically grown on plates containing 0.5x MS during 3 days. **(D)** Root length of oeOXR2 and *oxr2.2* plants grown in 0.5x MS medium supplemented with 0.1 µM MV during 10 DAS. **(E)** Root length of oeOXR2 and *oxr2.2* plants grown in 0.5x MS medium supplemented with 50 µM AA during 7 DAS**. (F)** Representative images of the phenotype of seedlings used for quantification of root length shown in (E)**. (G)** Representative images of the phenotype observed in seedlings grown in 1 µM MV during 6 days. Asterisks indicate significant differences at $P < 0.01$ (ANOVA, LSD Fisher test), using 20-40 plants of each genotype for the analysis.

Figure 9: Increased expression of At*OXR2* confers tolerance to high-light stress. (A) Photosynthetic parameters were measured in rosette leaves of oeOXR2 A and B plants grown under LD for 3 weeks and then exposed to HL (600 µE m^{-2} s^{-1}) during 3 days. RFU, relative fluorescence units. Results are expressed as mean±SD of five plants for each genotype. Asterisks indicate significant differences at $P < 0.05$ (ANOVA, LSD Fisher test). **(B)** Anthocyanin quantification was made using the whole rosette of oeOXR2 A and B lines grown under LD for 3 weeks and then exposed to HL for 3 days. **(C)** Expression levels of two genes involved in the anthocyanin synthesis pathway, *CHS* and *PAL*, analysed by RT-qPCR in triplicate pools of oeOXR2 A and B plants grown under LD for 3 weeks. **(D)** Ascorbic acid content in leaves of 3-week-old oeOXR2 (A and B) and WT plants. Results are expressed as mean±SD of five plants for each genotype. Asterisks indicate significant differences at $P < 0.01$ (*t*-test; Mann-Whitney test).

Figure 1

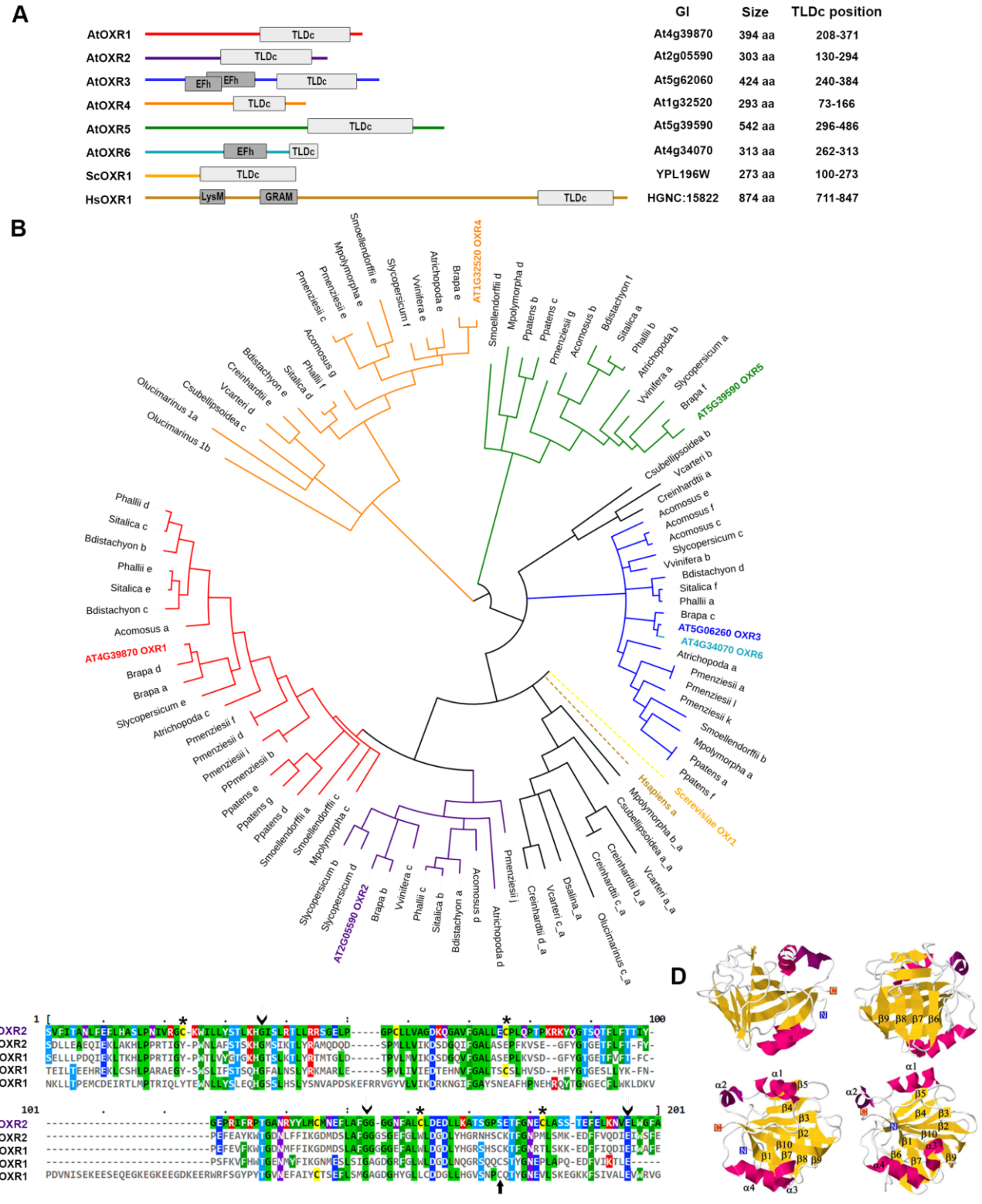

Figure 2

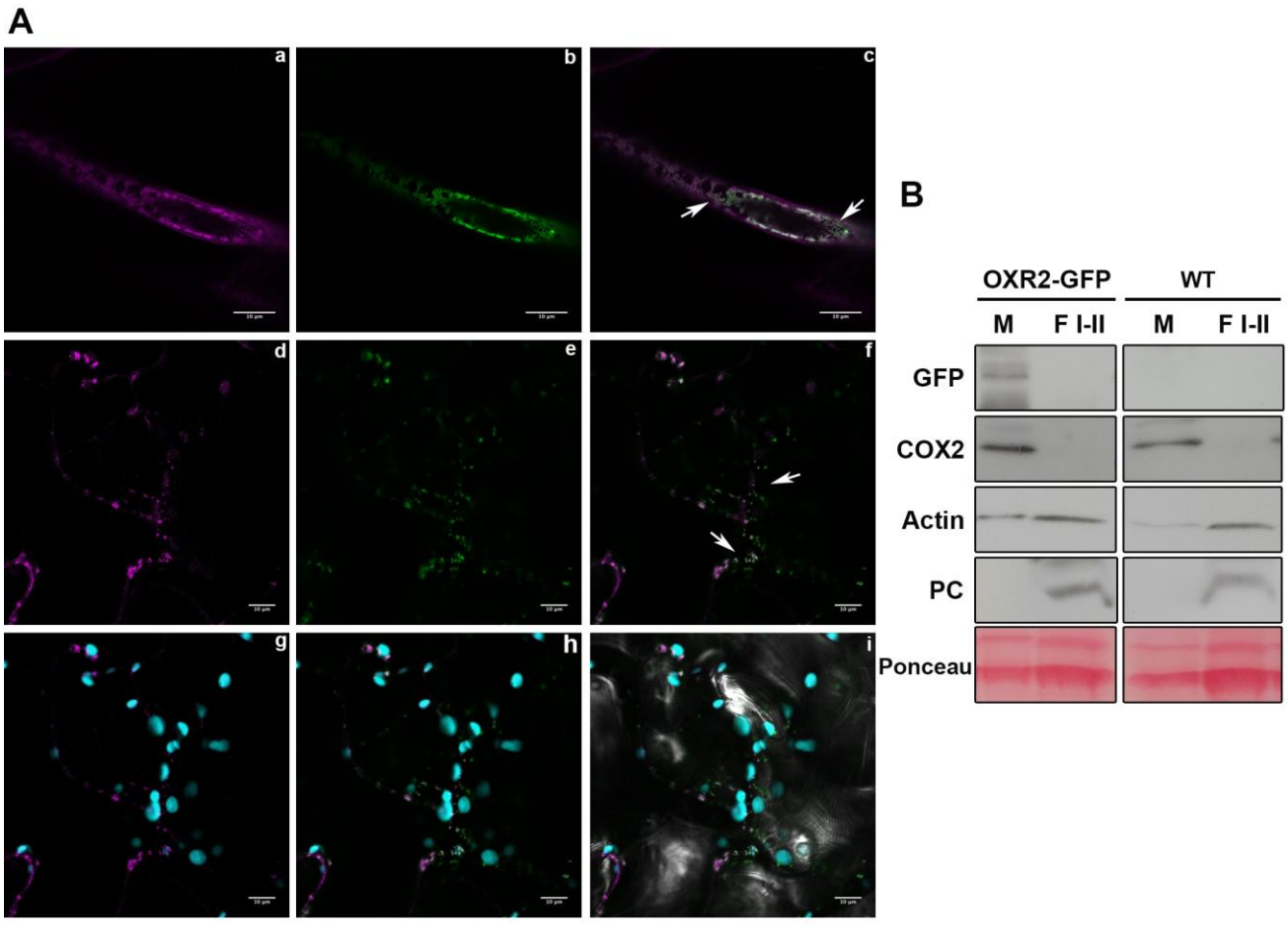

Figure 3

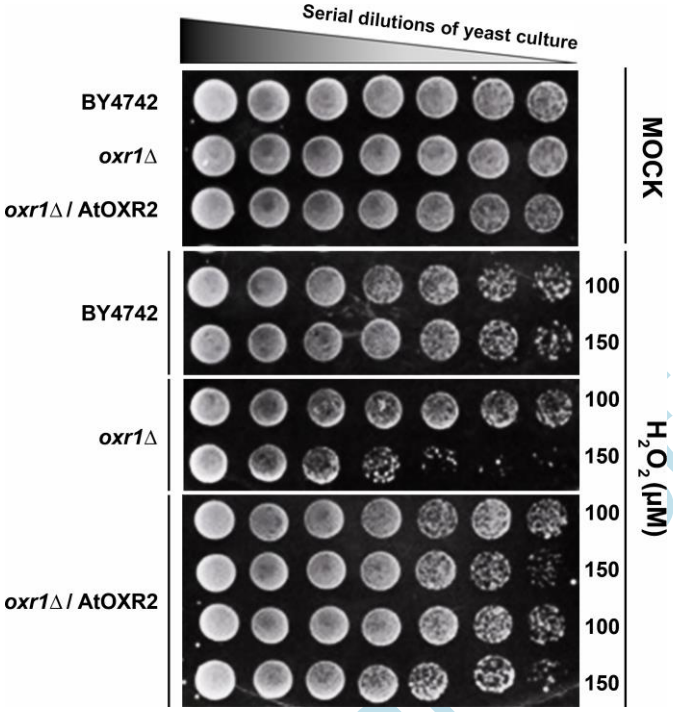

Figure 4

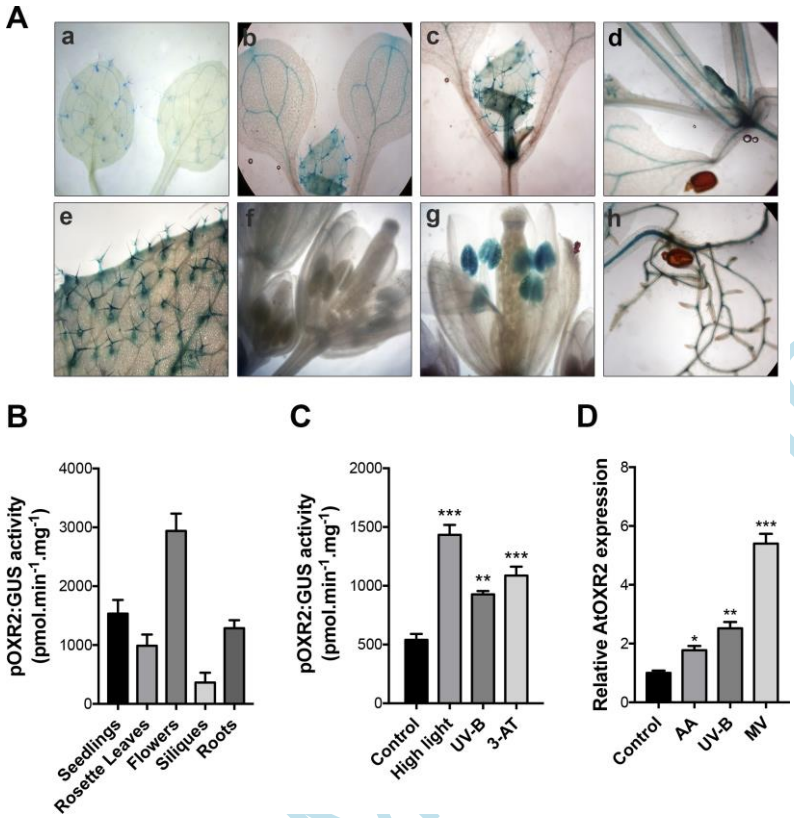

Figure 5

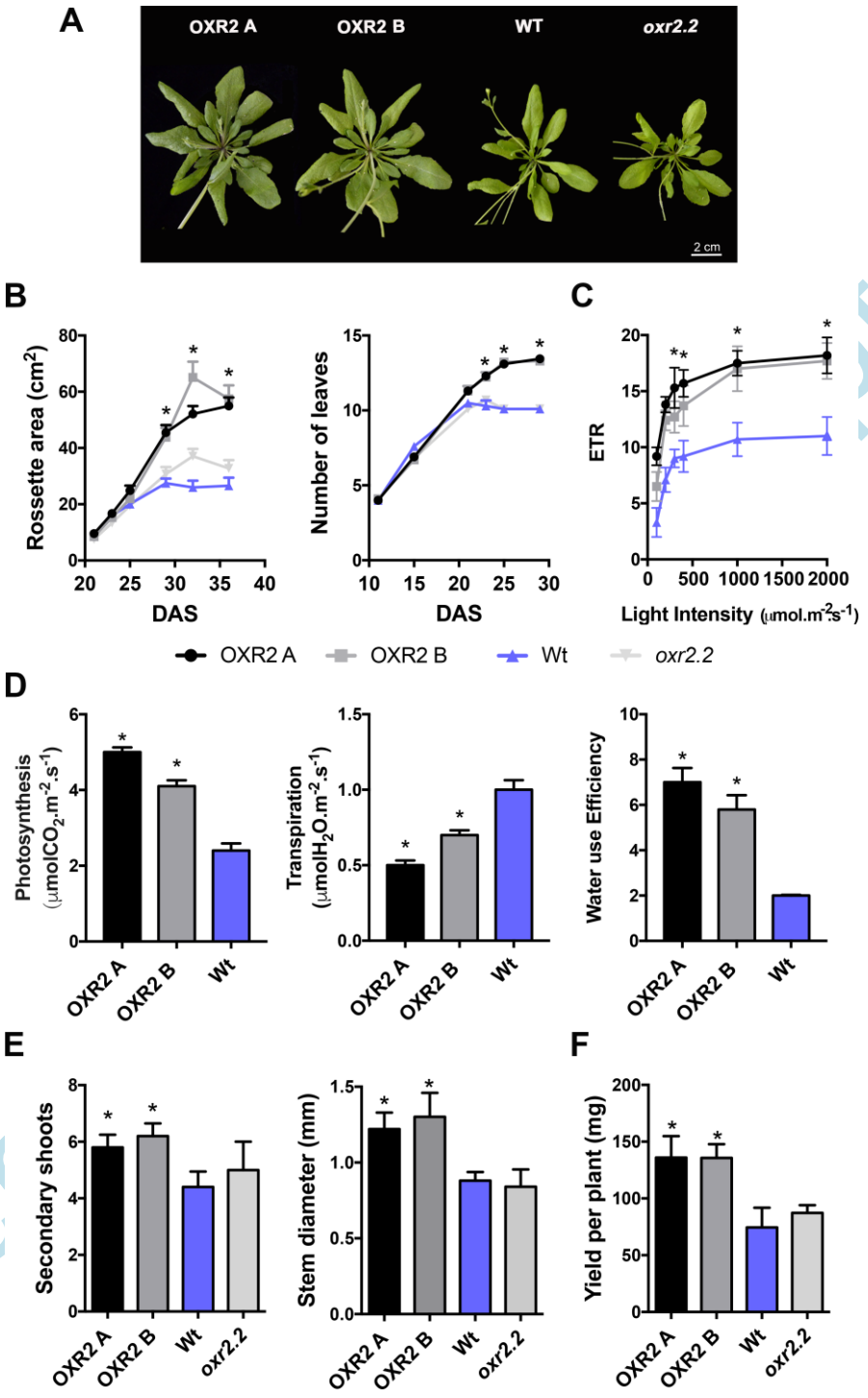

Figure 6

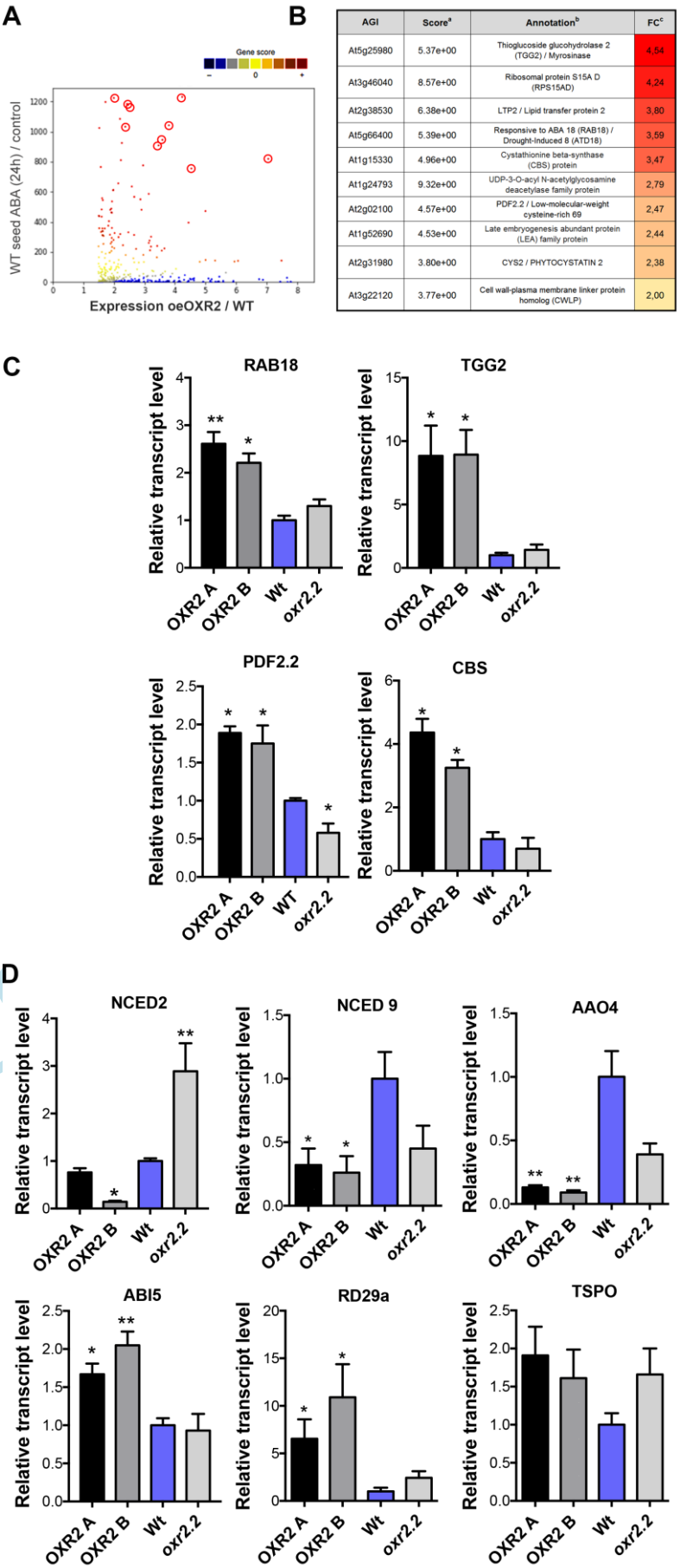

AGI	Score[a]	Annotation[b]	FC[c]
At5g25980	5.37e+00	Thioglucoside glucohydrolase 2 (TGG2) / Myrosinase	4,54
At3g46040	8.57e+00	Ribosomal protein S15A D (RPS15AD)	4,24
At2g38530	6.38e+00	LTP2 / Lipid transfer protein 2	3,80
At5g66400	5.39e+00	Responsive to ABA 18 (RAB18) / Drought-induced 8 (ATD18)	3,59
At1g15330	4.96e+00	Cystathionine beta-synthase (CBS) protein	3,47
At1g24793	9.32e+00	UDP-3-O-acyl N-acetylglycosamine deacetylase family protein	2,79
At2g02100	4.57e+00	PDF2.2 / Low-molecular-weight cysteine-rich 69	2,47
At1g52690	4.53e+00	Late embryogenesis abundant protein (LEA) family protein	2,44
At2g31980	3.80e+00	CYS2 / PHYTOCYSTATIN 2	2,38
At3g22120	3.77e+00	Cell wall-plasma membrane linker protein homolog (CWLP)	2,00

Figure 7

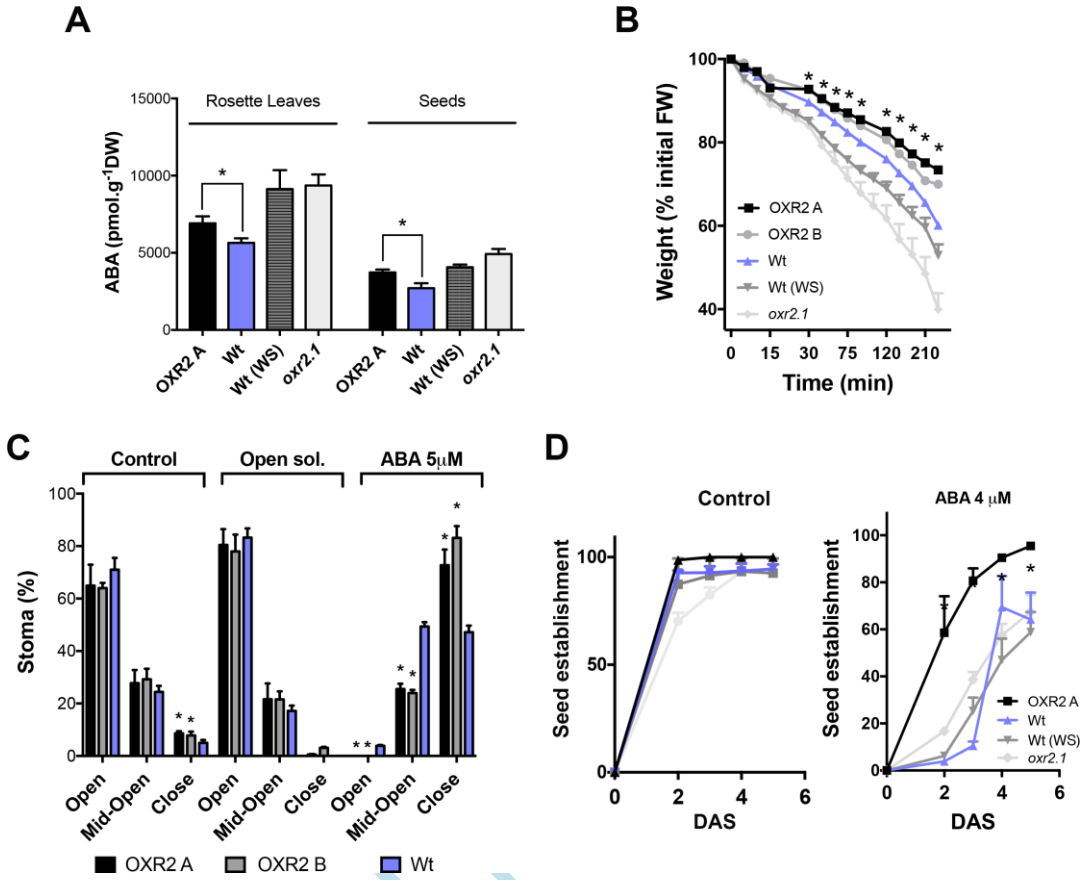

Figure 8

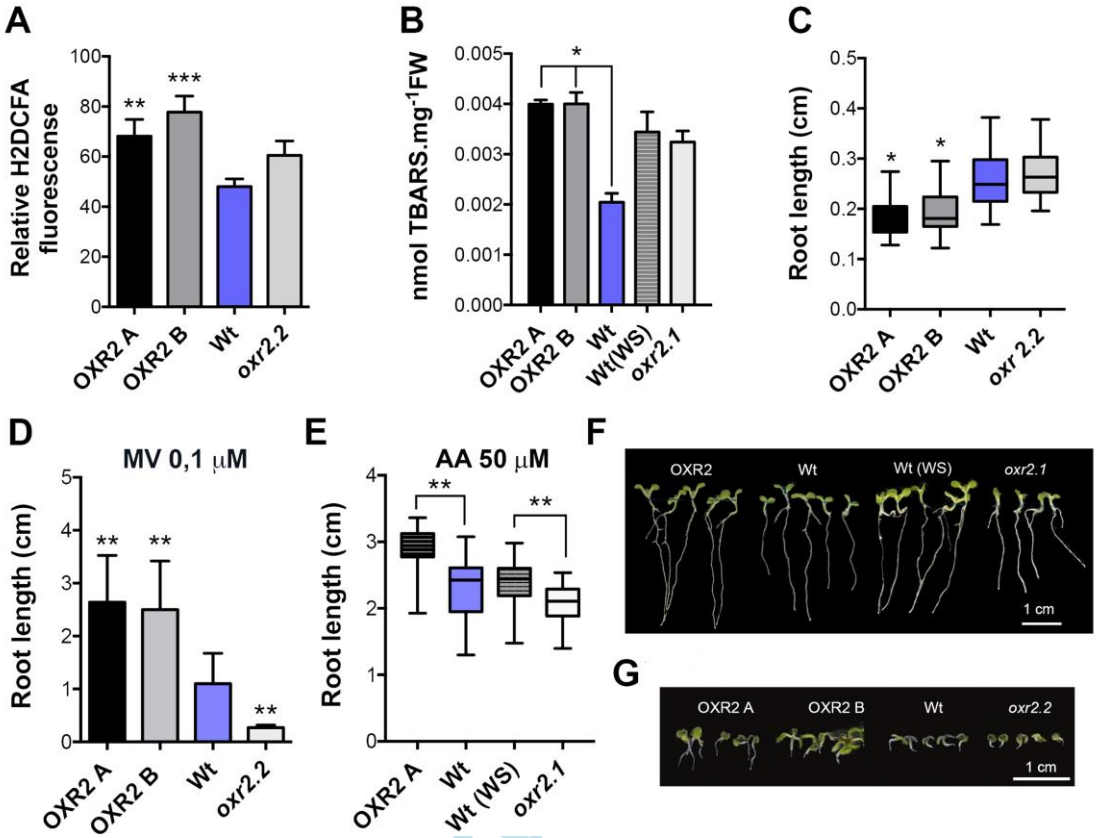

Figure 9